



HAL
open science

Neuropathological lesions in intravenous BCG-stimulated K18-hACE2 mice challenged with SARS-CoV-2

Lidia Sánchez-Morales, Néstor Porras, Teresa García-Seco, Marta Pérez-Sancho, Fátima Cruz, Blanca Chinchilla, Sandra Barroso-Arévalo, Marta Diaz-Frutos, Aránzazu Buendía, Inmaculada Moreno, et al.

► **To cite this version:**

Lidia Sánchez-Morales, Néstor Porras, Teresa García-Seco, Marta Pérez-Sancho, Fátima Cruz, et al.. Neuropathological lesions in intravenous BCG-stimulated K18-hACE2 mice challenged with SARS-CoV-2. *Veterinary Research*, 2024, 55 (1), pp.71. 10.1186/s13567-024-01325-7 . hal-04597535

HAL Id: hal-04597535

<https://hal.science/hal-04597535v1>

Submitted on 3 Jun 2024

HAL is a multi-disciplinary open access archive for the deposit and dissemination of scientific research documents, whether they are published or not. The documents may come from teaching and research institutions in France or abroad, or from public or private research centers.


L'archive ouverte pluridisciplinaire **HAL**, est destinée au dépôt et à la diffusion de documents scientifiques de niveau recherche, publiés ou non, émanant des établissements d'enseignement et de recherche français ou étrangers, des laboratoires publics ou privés.

RESEARCH ARTICLE

Open Access



Neuropathological lesions in intravenous BCG-stimulated K18-hACE2 mice challenged with SARS-CoV-2

Lidia Sánchez-Morales^{1,2†}, Néstor Porras^{1†}, Teresa García-Seco¹, Marta Pérez-Sancho^{1,2*} , Fátima Cruz¹, Blanca Chinchilla^{1,3}, Sandra Barroso-Arévalo^{1,2}, Marta Díaz-Frutos^{1,2}, Aránzazu Buendía¹, Inmaculada Moreno⁴, Víctor Briones^{1,2}, María de los Ángeles Risalde⁵, José de la Fuente^{6,7}, Ramón Juste⁸, Joseba Garrido⁸, Ana Balseiro⁹, Christian Gortázar⁶, Antonio Rodríguez-Bertos^{1,10}, Mercedes Domínguez⁴ and Lucas Domínguez^{1,2,11}

Abstract

In the wake of the COVID-19 pandemic caused by SARS-CoV-2, questions emerged about the potential effects of Bacillus Calmette-Guérin (BCG) vaccine on the immune response to SARS-CoV-2 infection, including the neurodegenerative diseases it may contribute to. To explore this, an experimental study was carried out in BCG-stimulated and non-stimulated k18-hACE2 mice challenged with SARS-CoV-2. Viral loads in tissues determined by RT-qPCR, histopathology in brain and lungs, immunohistochemical study in brain (IHC) as well as mortality rates, clinical signs and plasma inflammatory and coagulation biomarkers were assessed. Our results showed BCG-SARS-CoV-2 challenged mice presented higher viral loads in the brain and an increased frequency of neuroinvasion, with the greatest differences observed between groups at 3–4 days post-infection (dpi). Histopathological examination showed a higher severity of brain lesions in BCG-SARS-CoV-2 challenged mice, mainly consisting of neuroinflammation, increased glial cell population and neuronal degeneration, from 5 dpi onwards. This group also presented higher interstitial pneumonia and vascular thrombosis in lungs (3–4 dpi), BCG-SARS-CoV-2 mice showed higher values for TNF- α and D-dimer values, while iNOS values were higher in SARS-CoV-2 mice at 3–4 dpi. Results presented in this study indicate that BCG stimulation could have intensified the inflammatory and neurodegenerative lesions promoting virus neuroinvasion and dissemination in this experimental model. Although k18-hACE2 mice show higher hACE2 expression and neurodissemination, this study suggests that, although the benefits of BCG on enhancing heterologous protection against pathogens and tumour cells have been broadly demonstrated, potential adverse outcomes due to the non-specific effects of BCG should be considered.

Keywords BCG stimulation, SARS-CoV-2, K18-hACE2, neuroinvasion

Handling editor: Marie Galloux

[†]Lidia Sánchez-Morales and Néstor Porras contributed equally to this work and share the first authorship.

*Correspondence:

Marta Pérez-Sancho

maperezs@ucm.es

Full list of author information is available at the end of the article



© The Author(s) 2024. **Open Access** This article is licensed under a Creative Commons Attribution 4.0 International License, which permits use, sharing, adaptation, distribution and reproduction in any medium or format, as long as you give appropriate credit to the original author(s) and the source, provide a link to the Creative Commons licence, and indicate if changes were made. The images or other third party material in this article are included in the article's Creative Commons licence, unless indicated otherwise in a credit line to the material. If material is not included in the article's Creative Commons licence and your intended use is not permitted by statutory regulation or exceeds the permitted use, you will need to obtain permission directly from the copyright holder. To view a copy of this licence, visit <http://creativecommons.org/licenses/by/4.0/>. The Creative Commons Public Domain Dedication waiver (<http://creativecommons.org/publicdomain/zero/1.0/>) applies to the data made available in this article, unless otherwise stated in a credit line to the data.

Introduction

Severe acute respiratory syndrome coronavirus 2 (SARS-CoV-2) is the causative agent for the global pandemic of coronavirus disease 2019 (COVID-19), which resulted in 759 million confirmed cases and 6.8 million deaths reported as of 2023 [1]. COVID-19 is a multi-organ disease, that presents a diverse array of symptoms. It is important to note that a substantial 36.4% of individuals who succumbed to COVID-19 experienced neurological manifestations [2], including intracranial haemorrhages, parkinsonism, sleep disorders, and symptoms akin to Alzheimer's disease, such as cognitive deficits, seizures, delirium, and behavioral alterations [3]. Moreover, 30–60% of patients continue to experience neurological symptoms 6 months after their initial infection [4]. Additionally, individuals with pre-existing conditions such as Alzheimer's disease or autism are at higher risk of contracting COVID-19 due to potential disruptions with the blood–brain barrier, which can also exacerbate their underlying conditions, potentially leading to increased mortality rates [5].

The mechanism of SARS-CoV-2 infection involves the binding of the virus to the angiotensin-converting enzyme (ACE2) receptor present in human cells [6]. Although ACE2 receptors are distributed across various tissues, immunohistochemistry (IHC) studies revealed marked ACE2 staining in type I and II lung alveolar epithelial cells [7]. Notably, investigations of human brain tissue have identified the presence of hACE2 (human angiotensin-converting enzyme 2) receptors in vascular endothelial and smooth muscle cells, both in the peripheral and central nervous system [8, 9]. This finding offers one of the potential explanations for how the virus enters the brain and leads to neurological clinical symptoms and lesions [10].

The severity of COVID-19 clinical signs varies among individuals and is influenced by several factors, including age [11], sex [12], comorbidities with other diseases [13], and even blood type [14]. These variables can either exacerbate or mitigate the severity of the disease and its clinical manifestations. Another intriguing factor is the impact of prior immunization with immunomodulatory agents like the Bacillus Calmette–Guérin (BCG) vaccine, which has been suggested to play a role on the SARS-CoV-2 infection [15]. This is the only approved anti-tuberculosis vaccine which was originally developed to combat tuberculosis in the twentieth century and has been already administered worldwide in more than 4 billion doses [16]. Besides its primary function, BCG exhibits immunomodulatory properties and offers protection against diseases like leprosy, non-tuberculous mycobacterial lymphadenitis, and Buruli

ulcer [17]. It may also be associated with a lower risk on leukemia [18] and lung cancer [19], or a therapeutic effect bladder cancer [20]. Moreover, BCG induces trained immunity and non-specific protection against various infections, including respiratory tract infections and neonatal sepsis which protection can persist up to 1 year and involves increased production of proinflammatory cytokines [21].

The COVID-19 pandemic raised questions about whether BCG vaccination could enhance the immune response against SARS-CoV-2 [15, 22]. To explore this, population-based surveys studies were conducted [23, 24], suggesting that BCG vaccination may reduce the severity of COVID-19. However, there is some controversy, as other epidemiological studies identified BCG vaccination as a potential risk factor, increasing the likelihood of COVID-19 diagnosis, positive PCR tests, or hospitalization [25]. Similarly, certain studies have reported no decrease in SARS-CoV-2 infections [26]. In this way, the impact of BCG vaccination on COVID-19 remains uncertain and requires further investigation [27].

To address this uncertainty, the K18-hACE2 mouse model has emerged as a primary tool. These mice are transgenic and express the human hACE2 gene under the control of the cytokeratin-18 (k18) promoter [28]. This model has been frequently employed in initial investigations concerning the pathogenesis of SARS and SARS-CoV-2, as well as in the development of vaccines against these diseases [29]. However, it is important to consider the higher expression of ACE2 receptors and viral neurodissemination observed in this model in comparison to humans [30]. Recent research has explored brain lesions in K18-hACE2 transgenic mice resulting from SARS-CoV-2 infection and brain invasion, examining viral replication [31] and the chronological progression of histological lesions [32]. Additionally, many studies have explored the distribution of SARS-CoV-2 antigen and the impact on the olfactory bulb, as well as presence of anosmia in k18-hACE2, a common sign in human disease [33]. The results regarding BCG stimulation in this experimental model have been diverse, with some studies suggesting beneficial effects [30, 34] while others reported no discernible protection against SARS-CoV-2 [35, 36]. Other experimental models such as golden Syrian hamster have been also utilized, showing positive results for BCG vaccination in reducing the severity of SARS-CoV-2 infection [37]. A gap remains in the literature, as studies that integrate BCG administration prior to SARS-CoV-2 infection along with comprehensive histopathological study of brain lesions are lacking. This highlights a significant research void to clarify the potential association between BCG stimulation and neurological diseases together

with SARS-CoV-2 infection, since BCG has already been related to some therapies against neurological illnesses [38].

The present study was conducted to offer a comparative analysis of the disease's progression and central nervous system lesions as well as the effects BCG may have in both.

To our knowledge, this investigation contributes to the field with a comprehensive brain histopathological and IHC evaluation of BCG-stimulated K18-hACE2 mice post-SARS-CoV-2 challenge, providing new insights in this research area.

Materials and methods

Animals

Animal care and procedures were performed by following the guidelines of good experimental practices according to Directive 2010/63/EU of the European Parliament and of the Council of 22 September 2010 on the protection of animals used for scientific purposes [amended by the Regulation (EU) 2019/1010] and Spanish laws (RD 53/2013). The protocol was approved by the Community of Madrid Ethics Committee (reference PROEX 180.2/22). K18-hACE2 male and female mice ($n=43$) aged 4–6 weeks were obtained from Charles River Laboratories (Wilmington, Massachusetts, USA). The cages were equipped with Altromin-LASQCdiet[®] Rod 14-H (Altromin Lage, Germany) for feeding. Both food and water were available ad libitum. Wheeled houses for environmental enrichment were also included (Ref: K3327+K3250, Sodispan Research, Madrid, Spain). During the initial 10 day-period, they were given time to acclimate to their new cages and socialize with their partners. After that period, the animals were marked with an ear tagger for individual identification (in many cases, it was not necessary since mice were easily identifiable by white areas on their tails). BCG administration procedures were carried out in the Biosafety Level 2+ (BSL2+) area at the VISAVET Health Surveillance Centre (Complutense University, Madrid). Thirty days after immunization, animals were moved to the Biosafety Level 3 (BSL3) area at the VISAVET Centre for SARS-CoV-2 infection studies.

SARS-CoV-2 virus and cell lines

SARS-CoV-2 MAD6 was used for experimental infection assay. Calu 3 cells were prepared to reproduce stocks of SARS-CoV-2 [39]. The cells were incubated at 37 °C under 5% CO₂ in Eagle's Minimum Essential Medium (EMEM) with L-glutamine (Merck KGaA, Darmstadt, Germany) and supplemented with 100 IU/mL penicillin, 100 µg/mL streptomycin, and 10% fetal bovine serum (FBS) (Merck KGaA, Darmstadt, Germany).

For viral growth in Calu-3 cells, a multiplicity of infection (MOI) of 0.0001 was used. After the virus was absorbed for one hour at 37 °C, the viral growth media EMEM supplemented with 2% fetal bovine serum was added. The cell lysate and supernatant were harvested after 3 days of incubation at 37 °C with 5% CO₂.

Vero E6 cells, provided by the Carlos III Health Institute (Madrid, Spain), or ATCC[®] (Manassas, Virginia, USA), were prepared to titrate SARS-CoV-2 stocks by determining the amount of virus causing cytopathic effects in 50% of tissue culture infectious dose (TCID50/mL). Additionally, this cell line was used to verify the viability of the SARS-CoV-2 inoculum used for infecting the animals.

BCG preparation

BCG was inoculated in a starter liquid culture with a vial of frozen strain, incubated at 37 °C in aerobiosis for 4 weeks and then inoculated in a liquid culture at 37 °C in aerobiosis for another 4 weeks. At the end of the culture, the growth was collected with a pipette, centrifuged, washed with PBS and given a treatment of physical breakage with glass beads, and diluted with PBS until a homogeneous product was at approximately 1 McFarland [equivalent to approximately 10⁶ colony forming units (CFU)/mL]. Once the inoculum was ready, a plate count was performed to determine the concentration of the prepared inoculum, as well as afterwards the inoculation of BCG in the mice. The final dose for inoculation obtained was 1.3×10⁵ CFU in 100 µL at a concentration of 1.3×10⁶ CFU/mL.

Experimental design

Animals were divided into 3 different experimental groups: Group 1, "only challenged with SARS-CoV-2" (SARS-CoV-2, $n=22$; 13 females and 9 males); Group 2, "BCG-stimulated and SARS-CoV-2 challenged" (BCG-SARS-CoV-2, $n=21$; 12 females and 9 males); Group 3 "non-stimulated, nor challenged" (negative control animals, $n=4$; 2 females and 2 males) (Figure 1, Additional file 1). Groups 1 and 2 were divided into two subgroups follow-up duration: (i) animals sacrificed at 3–4 days post-infection (dpi), (ii) animals that developed COVID-19 and were sacrificed when they reached the endpoint criteria described in the following section (5, 6, 7 dpi), or animals left until the 8 dpi (end of the experiment) that did not develop COVID-19 or did not reach endpoint criteria.

BCG administration, SARS-CoV-2 infection, and sampling

BCG was intravenously (IV) administered using a syringe with a 30 G needle through the caudal vein of the tail (group 2, Figure 1). A restrainer was used to

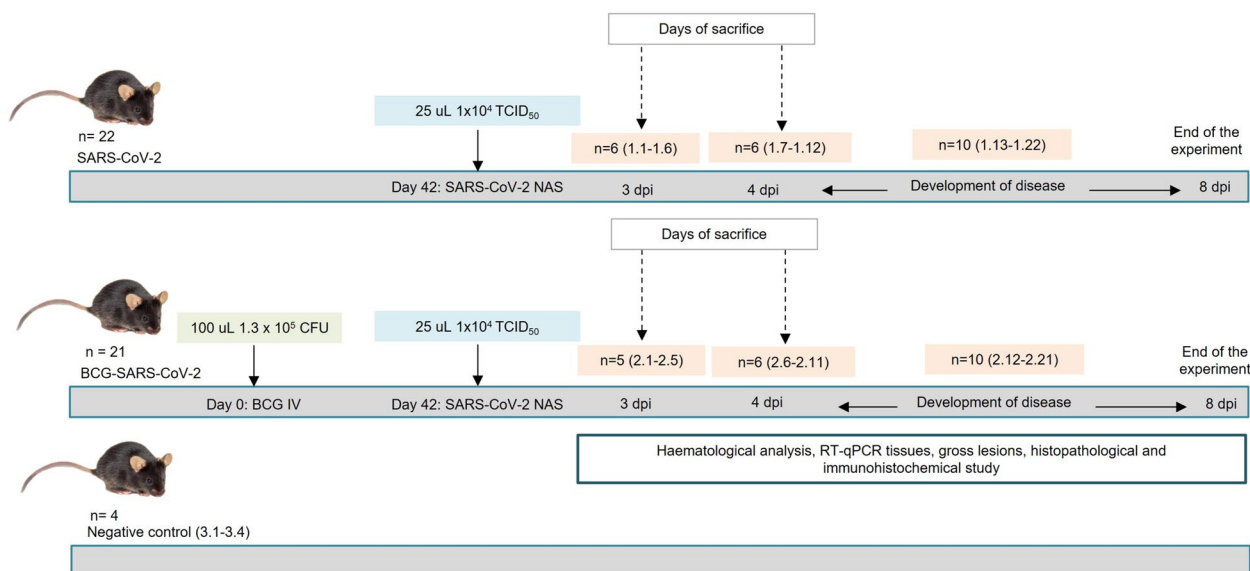


Figure 1 Experimental design and timeline, depicting the immunization-to-sacrifice period for the three different groups of animals included in the study. Group 1 (animals challenged with SARS-CoV-2 only, named SARS-CoV-2, $n = 22$; 13 females and 9 males), Group 2 (animals intravenously administered BCG and challenged with SARS-CoV-2, named BCG-SARS-CoV-2, $n = 21$; 12 females and 9 males), Group 3 (negative control animals which were neither BCG-stimulated nor SARS-CoV-2 challenged, named control, $n = 4$; 2 females and 2 males).

immobilize the mouse while administering BCG. The tail was pre-warmed slightly using a heat lamp for enhanced vasodilation. Animals were challenged with the SARS-CoV-2 virus 6 weeks after the intravenous BCG administration (Figure 1).

For infection, the 43 mice (groups 1 and 2) were sedated with xylazine (20 mg/mL) at a dose of 2 mg/kg and ketamine 100 mg/mL at a dose of 20 mg/kg intraperitoneally (IP). Afterwards, animals were inoculated intranasally (NAS) with SARS-CoV-2 at a dosage of 1×10^4 TCID₅₀ per mouse. The total volume inoculated was of 25 μ L alternating nostrils in volumetric fractions of 5 μ L (Figure 1).

To confirm that animals were successfully infected (groups 1 and 2), oropharyngeal swab samples were

collected at 2 dpi [DeltaSwab[®] Virus with viral transport media (MTV) (Deltalab S.L, Cataluña, Spain)]. In addition, a COVID19 dtec RT-qPCR Test (Genetic PCR Solutions[™], Alicante, Spain) test was carried out to quantify the infection inoculum with a result of 1.94×10^6 copies/ μ L.

Following the challenge, animals were weighed and monitored daily for clinical signs. A clinical scoring table (Table 1) was prepared and utilized to document each clinical sign on a scale from 0 to 2. The animals were sacrificed upon reaching a cumulative clinical score (sum of scores for each evaluated clinical sign) of 4 or a loss of weight higher than 20%. Once the designated sacrifice days were reached (3 and 4 dpi), or endpoint criteria was fulfilled, blood samples in heparin were obtained from

Table 1 Score of the different clinical signs analyzed throughout the experience since the infection of the animals

Clinical score	0	1	2
Loss of weight	None/slight (0–10%)	Moderate (10–20%)	Severe (> 20%)
Hair appearance	Undamaged	Slightly tousled	Bristly
Level of activity	Normal	Reduced activity	Inactive
Eye closing	Normal eyes	Slightly bent	Totally closed
Respiratory signs	Normal	Slightly increased	Tachypnoea, dyspnoea or abdominal tightening
Neurological signs	None	Depression, bending posture, difficulty in walking	Tremors or convulsions

the animals after sedation IP with xylazine (20 mg/mL) at a dose of 4 mg/kg and ketamine (100 mg/mL) at a dose of 40 mg/kg, before sacrifice. The animals that did not meet the endpoint criteria were euthanized on day 8 post-infection, marking the end of the experiment. Subsequently, a comprehensive necropsy was conducted on the animals. In this study, brain, lung, trachea, and nasal turbinates samples were collected in AllProtect Tissue Reagent (Qiagen, Venlo, Netherlands) for viral RNA detection. Brain and lung tissues were also collected in 10% neutral formalin for histopathology and IHC studies.

SARS-CoV-2 RNA extraction and reverse transcription-quantitative PCR (RT-qPCR)

AllPrep[®] DNA/RNA/Protein Mini Kit (Qiagen, Venlo, Netherlands) was used for RNA extraction of tissues according to the manufacturer's instructions. In addition, the detection and quantification of SARS-CoV-2 loads from tissues and swabs was performed using the CoVID19 dtec RT-qPCR Test (Genetic PCR Solutions[™], Alicante, Spain).

Measurements of inflammatory and coagulation markers

Complete heparinized blood was centrifugated and plasma was stored at -80°C until the analyses of the following biomarkers: CRP (C-reactive protein) (Mouse CRP ELISA Kit. Invitrogen, Massachusetts, USA), ferritin (Mouse Ferritin ELISA kit. Crystal Chem, Zaandam, Netherlands), D-dimer [Mouse D2D (D-Dimer) ELISA Kit. FineTest[®], Boulder, USA] and iNOS (nitric oxide synthase) (iNOS ELISA Kit. MyBioSource, San Diego, USA).

Proinflammatory cytokines as interleukin 1 β (IL-1 β), interleukin 6 (IL-6), tumour necrosis factor alpha (TNF- α), interferon gamma (IFN- γ), and anti-inflammatory as interleukin 1 receptor antagonist (IL-1ra) and transforming growth factor beta-1 (TGF- β 1) were measured with the Ella[™] Automated Immunoassay System (ProteinSimple, Abingdon, Belgium).

Histopathological and immunohistochemical evaluation

The lung and brain were fixed in 10% neutral formalin for 48 h. The samples were automatically processed

(Citadel 2000 Tissue Processor, Thermo Fisher Scientific, Waltham, MA, USA) and embedded in paraffin (HistoStar Embedding Workstation, Thermo Fisher Scientific). Five consecutive sections of 4 μm thickness were obtained for each case using a microtome (FinesseMe+, Thermo Fisher Scientific). One section was stained with haematoxylin–eosin (HE) (Gemini AS Automated Slide Stainer, Thermo Fisher Scientific) and the following four sections were placed in positively charged glass slides and used for further immunohistochemical studies.

The paraffin sections placed in positively charged glass slides were deparaffinised in xylene and rehydrated. This step was carried out by the EpreDia PT module Deparaffin and Heat Induced Epitope Retrieval (HIER) (Thermo Fisher Scientific). Endogenous peroxidase was blocked by immersing the samples in a 3% hydrogen peroxide in methanol solution (Panreac Química S.L.U, Spain) for 15 min. Then, the samples were incubated with 2.5% Normal Horse Serum for blocking (RTU) for 1 h. Afterwards, the slides were subsequently incubated overnight at 4°C with the primary antibodies detailed in Table 2 (Thermo Fisher Scientific; DAKO, Glostrup, Denmark). Positive and negative controls were included in each batch of slides. For negative controls, the primary antibody was omitted and substituted by tris-buffered saline. After night, secondary antibody was added (ImmPRESS[®] VR Horse AntiMouse IGG Polymer Kit, Peroxidase; Vector Laboratories, Newark, California, United States) and incubated for 1 h. For the revealing process peroxidase was used (ImmPACT[®] NovaRED[®] Substrate Kit Peroxidase; Vector Laboratories, Newark, California, USA). Finally, samples were mounted (CTM6 Coverslipper, Thermo Fisher Scientific) and evaluated for histopathological alterations under a Leica DM2000 microscope (Leica Microsystems, Wetzlar, 162 Germany).

Pulmonary histological score was derived from the assessment of 14 parameters across different experimental groups with the objective of characterizing the lung injury severity: pleuritis, septal thickening, peribronchiolar inflammatory cell infiltration, perivascular inflammatory cell infiltration, oedema, desquamative alveolitis, atelectasis, emphysema, type II pneumocytes hyperplasia, bronchiolar hyperplasia,

Table 2 List and details of antibodies used in the immunohistochemical study

Antibody	Type	Host	Dilution	Company
Anti-SARS-CoV-2	Monoclonal	Mouse	1:100	Thermo Fisher Scientific
Anti-CD3	Polyclonal	Rabbit	1:100	DAKO
Anti-PAX5	Monoclonal	Mouse	Ready to use	DAKO
Anti-Iba-1	Polyclonal	Rabbit	1:50	Thermo Fisher Scientific

vasculitis, perivascular oedema, haemorrhage, and thrombosis. Each histopathological parameter was evaluated according to a 3-point scale from 0 to 3 indicating: 0 no lesion, 1 mild lesion, 2 moderate lesion, and 3 severe lesions. Mean values and standard deviations of histopathological parameters were calculated for each mouse and for each group of mice.

Histopathological and immunohistochemical scorings were performed in the following brain sections: olfactory bulb, pyriform cortex, septum-striatum, cerebral cortex, hippocampus, thalamus, hypothalamus, mesencephalon, pons, cerebellum, and spinal cord. The parameters assessed were perivascular lymphocytic cuffing, vasculitis, perivascular haemorrhage, thrombosis, shrunken neurons, neuropil spongiosis (cytoplasmic ballooning), white matter tract myelin sheath vacuolation, microglial activation (neuronophagia), oligodendrocyte activation (satellitosis), astroglial activation (astrogliosis). Paxinos and Franklin atlas [40] was consulted for histological identification of the different brain regions. Parameters were scored from 0 to 5 according to their degree of severity, based on the proportion of affected cells/tissue (Table 3). The range score for histopathology goes from 0 to 570 in each animal; one animal was considered affected when it showed a score value higher than 20 (since it was the highest score in negative control animals—group 3—assuming it could be due to artifacts and unspecific lesions). With respect to IHC, SARS-CoV-2 neuronal immunoreexpression were scored from 0 to 5 according to their degree of extension, based on the proportion of infected neurons (Table 3); the range score goes from 0 to 55 (Table 3).

Statistical analysis and graphic creation

Odds ratios and Risk Ratios/Relative risks were performed using MedCalc for Windows, version 22.014 (MedCalc Software, Ostend, Belgium).

Correlation between the detection of SARS-CoV-2 in the lung and brain was estimated with Spearman's Rho coefficient in IBM SPSS Statistics for Windows,

version 287.0. 1. 1 (15) (IBM Corp, Armonk, N.Y, USA). Differences between groups regarding to qualitative variables (proportion of PCR-positive brain samples) were tested using Fisher's test in SPSS. Differences between groups regarding to quantitative variables (viral loads in organs, histopathological brain and lung lesions, cytokine measurements and hematological inflammation markers) were evaluated using Kruskal–Wallis test and Mann–Whitney test in SPSS. Mann–Whitney *p*-values were adjusted according to FDR (False Discovery Rate). Statistically significant differences in all tests were considered when *p*-value was < 0.05.

Figures 2, 3 and 6 were created using GraphPad Prism 10 software.

ChatGPT was used on some occasions to improve the drafting of the article.

Results

BCG-stimulated SARS-CoV-2 challenged animals presented higher viral loads in brain than not stimulated mice

The study of the disease progression as well as the measurement of viral loads are valuable tools to learn about the development of the disease in different experimental groups assessing the influence of BCG stimulation before SARS-CoV-2 infection. The number of PCR-positive animals in brain samples was significantly higher in BCG-SARS-CoV-2 challenged mice (Fisher's test, *p* = 0.034). In group 1 (SARS-CoV-2), 5 mice out of 22 (22.7%) tested positive in brain RT-qPCR from 5 dpi onward. The animal with the highest brain viral load in this group, was found dead on 7 dpi (Additional file 1). In the BCG-SARS-CoV-2 mice (group 2), 14 out of 21 mice (66.6%) tested positive for brain RT-qPCR, being the highest viral load of an animal euthanized at 6 dpi (2.13). The highest brain viral loads were observed in animals euthanized at 6–7 dpi, coinciding with the highest clinical scores (Figure 2, Additional file 1). No animal euthanized at 8 dpi from any of the groups showed brain viral loads.

Group 2 (BCG-SARS-CoV-2) had significantly higher brain viral loads than group 1 (SARS-CoV-2)

Table 3 Evaluation criteria for histopathologic and immunohistochemical scoring (SARS-CoV-2 immunoreexpression) according to the amount of nervous tissue affected, classifying the lesions into 5 levels

	Histopathological score		Immunohistochemical score	
Negative	0% affected tissue/cells	0	Negative	0
Minimal	0–20% affected tissue/cells	1	Focal (single neuron)	1
Mild	20–40% affected tissue/cells	2	Oligofocal (single neuron)	2
Moderate	40–60% affected tissue/cells	3	Focal (neuron aggregates)	3
Marked	60–80% affected tissue/cells	4	Multifocal (neuron aggregates)	4
Severe	80–100% affected tissue/cells	5	Multifocal to coalescing/diffuse (neuron aggregates)	5

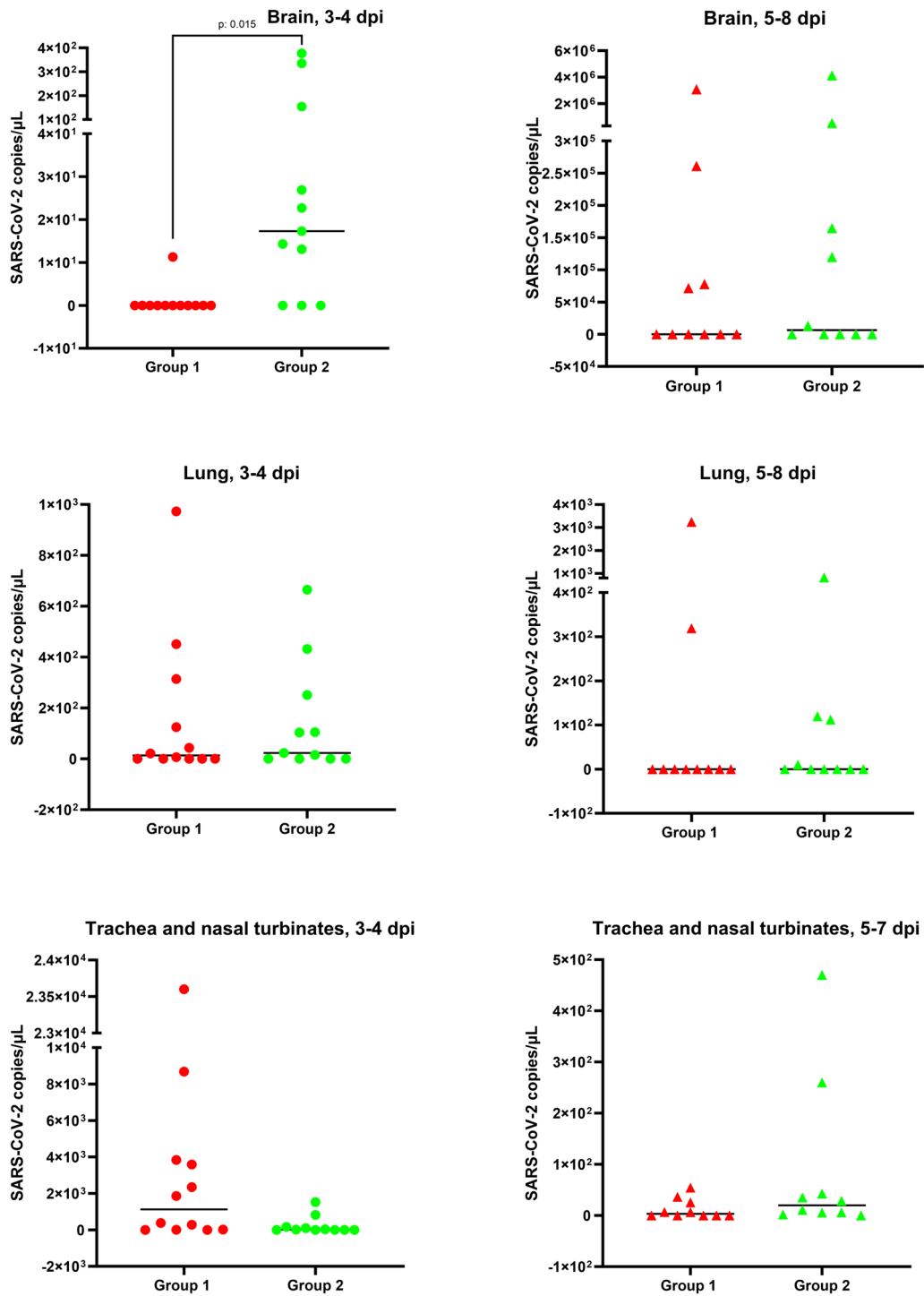


Figure 2 Plot representation of PCR results for each animal from group 1 (SARS-CoV-2) and group 2 (BCG-SARS-CoV-2). These groups are separated in two different subgroups: (i) 3–4 dpi and (ii) development of disease. Brain, lung, and trachea/nasal turbinates viral loads (copies/μL of purified RNA) are depicted with red (group 1, dots for 3–4 dpi, triangles 5–8 dpi) and green (group 2, dots for 3–4 dpi, triangles for 5–8 dpi). The SARS-CoV-2 loads (copies/μL) from brain, lung and trachea/nasal turbinates are shown. The limit of detection cutoff for the PCR corresponded to 2 copies/μL. The horizontal bars represent the median of the values for each group.

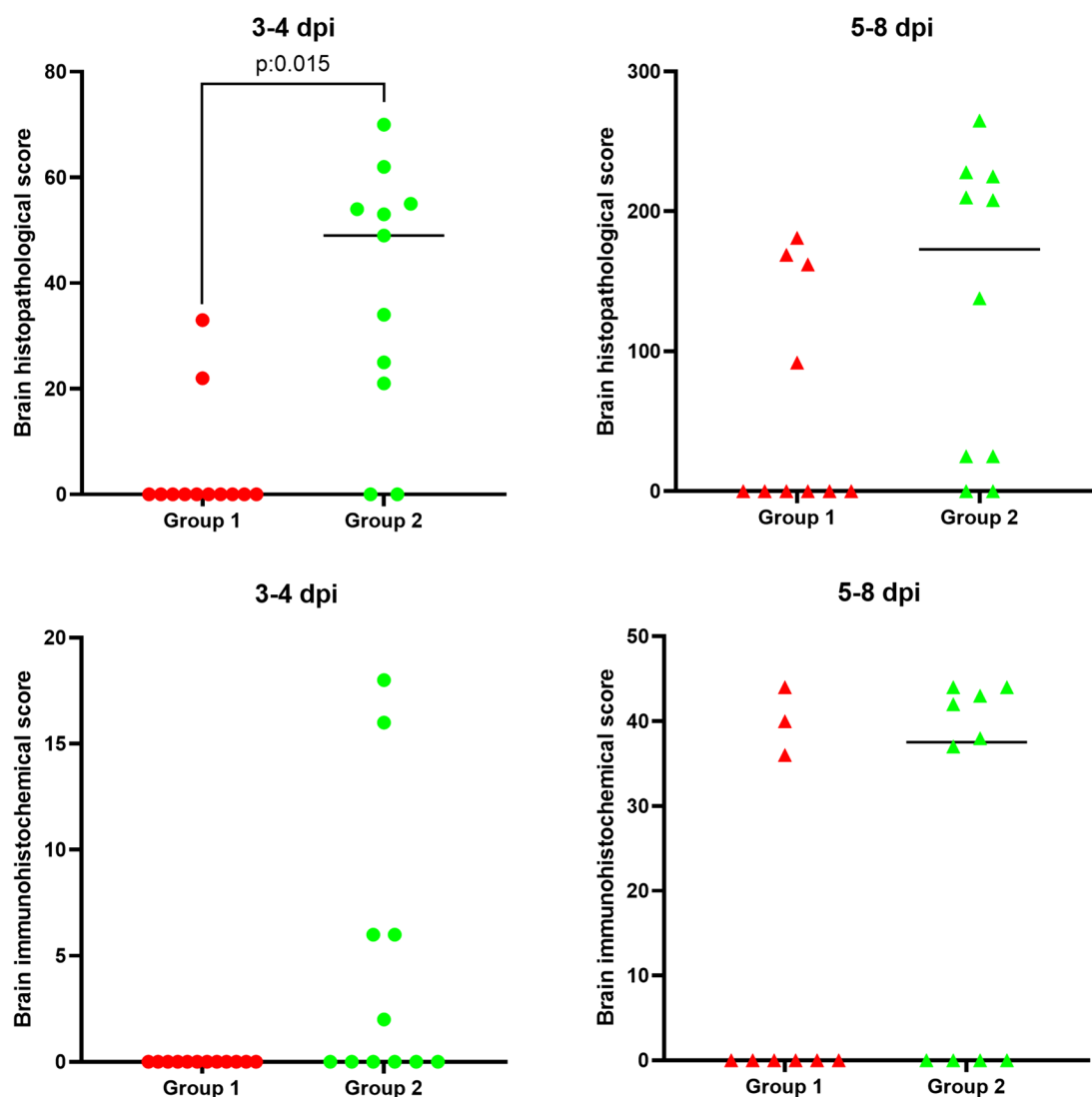


Figure 3 Plot representation of results for each animal from group 1 (SARS-CoV-2) and group 2 (BCG-SARS-CoV-2). These groups are separated in two different subgroups: (i) 3–4 dpi and (ii) development of disease. Brain histopathological and immunohistochemical score are depicted with red (group 1, dots for 3–4 dpi, triangles 5–8 dpi) and green (group 2, dots for 3–4 dpi, triangles 5–8 dpi). The horizontal bars represent the median of the values for each group.

(Mann–Whitney test, $p=0.042$). These differences were focused at 3–4 dpi ($p=0.015$) while no significant differences were observed at 5–8 dpi (Figure 2).

The RT-qPCR was also performed on lung, nasal turbinate, and trachea samples. In lungs, similar viral loads between groups were obtained (mean copies/ μL group 1=0.40, SD=0.50; mean group 2=0.52, SD=0.51). No significant differences were observed either in the RT-qPCR results for lungs between both groups (Mann–Whitney test, $p=0.821$) (Figure 2). The highest lung viral loads were observed between 3 and 7 dpi, while at 8 dpi no viral loads were detected. A positive correlation was observed between the detection

of SARS-CoV-2 in the lung and brain (Spearman’s Rho coefficient=0.375; $p=0.013$). Regarding nasal turbinate and trachea samples, viral RNA only persisted in BCG-SARS-CoV-2 animals until 8 dpi (Figure 2).

In group 1 (SARS-CoV-2), a morbidity rate of 40% was observed (4 out of 10 mice presented clinical signs and were sacrificed), while in mice belonging to group 2 (BCG-SARS-CoV-2), the morbidity rate after SARS-CoV-2 infection was 60% (6 out of 10 mice) (OR=2.25 95% CI=0.37–13.46). The challenged animals that remained clinically healthy were sacrificed on the last day of the experiment (8 dpi). Animals started to show clinical signs from 5 dpi onwards, with the most observed

signs being reduced activity and weight loss (3 animals in group 1 and 6 animals in group 2). At the time of death (5–7 dpi), the median clinical score was of 5 ± 0.87 (Additional file 1).

BCG stimulation increased the severity of SARS-CoV-2-induced brain lesions

Neuroinvasion and dissemination are key to the fatal development of SARS-CoV-2 in this experimental model [41]. For these reasons, histopathological and IHC studies were carried out. Animals from BCG-SARS-CoV-2 group (group 2) exhibited significantly more severe brain lesions due to SARS-CoV-2 infection in comparison to mice from group 1, as demonstrated by histological analysis (Mann–Whitney test, $p=0.001$) (Figure 3).

Meningoencephalitis was characterized by leptomeningeal mononuclear infiltrates and perivascular cuffs (T lymphocytes), with increased glial cell population, mainly microglia and astrocytes. No relevant inflammatory brain lesions were observed at 3 dpi, except for one BCG-SARS-CoV-2 case (group 2, 1/5 cases; histopathological score (HS) range=8–31). At 4 dpi, mild non-suppurative meningoencephalitis was infrequently observed in both BCG-SARS-CoV-2 (group 2, 2/6 cases; HS range=12–41) and SARS-CoV-2 (group 1, 1/6 cases; HS range=3–19) groups. A notable shift in lesion severity occurred from 5 dpi onwards, affecting almost the entire brain (except for the cerebellum), and cervical spinal cord. At 6–7 dpi, non-suppurative meningoencephalitis reached its maximum severity, with a statistically significant higher histopathological score in BCG-SARS-CoV-2 group (5/5 cases; HS range=107–143) compared to SARS-CoV-2 group (3/3 cases; HS range=95–107) (Mann–Whitney test, $p=0.036$) (Figure 4).

Vascular alterations included lymphoplasmacytic infiltration into the vascular wall (vasculitis), occasional obstruction due to degenerated erythrocytes attached to the vascular wall, and perivascular microhaemorrhages in both grey and white matter, as well as in the subarachnoid space. Minimal vascular alterations were observed at 3 dpi in both BCG-SARS-CoV-2 (group 2, 3/5 cases HS range=1–11) and SARS-CoV-2 groups (group 1, 1/6 cases; HS range=1–6). At 4 dpi, the BCG-SARS-CoV-2 group (4/6 cases; HS range=2–22) in terms of mild vasculitis and microhaemorrhages showed a relative risk of 4.6 (HE 95% CI=0.69–31.22) compared to group 1 (1/6 cases; HS range=1–5). At 5 dpi, the severity of vasculitis and haemorrhages increased, reaching their maximum severity at 6–7 dpi. Hyaline thrombi deposition at the vascular wall was observed to a lesser extent. These vascular alterations were more severe in BCG-SARS-CoV-2 animals (5 cases; HS range=29–55)

than in SARS-CoV-2 animals (3 cases; HS range=26–34) (Mann–Whitney test, $p=0.053$).

At 3–4 dpi, mild neuronal alterations were observed in BCG-SARS-CoV-2 group (7/11 cases; HS range=3–18) and minimally in SARS-CoV-2 group (2/12 cases; HS range=4–6) (Figure 4). These alterations included the presence of red shrunken neurons, adjacent to areas of increased glial cell population and vascular damage. At 4 dpi, swollen neurons with cytoplasmic ballooning and pyknotic and eccentric nuclei (neuronal degeneration) began to appear in both groups. These findings were prevalent in several brain regions and the spinal cord at 5 dpi. The maximum expression of lesions was observed at 6–7 dpi, with extensive neuronal degeneration. Bilateral and symmetrical myelin sheath vacuolation was displayed in the white matter tracts, affecting major myelin-rich areas. Neuronal alterations were more frequent and significantly more severe in BCG-SARS-CoV-2 animals (5 cases; HS range=54–80) than in SARS-CoV-2 animals (3 cases; HS range=40–47) (Mann–Whitney test, $p=0.024$) (Figure 4). Animals sacrificed at 8 dpi had no significant lesions. Additional file 2 shows more detailed information concerning histopathological score results.

Increased neuroinvasion and interneuronal dissemination of SARS-CoV-2 antigen in BCG-stimulated animals

BCG-SARS-CoV-2 animals (group 2) showed a relative risk of developing brain lesions due to SARS-CoV-2 at 3–4 dpi of 4.9 (HE 95% CI=1.34–17.93) and 11.9 (IHC 95% CI=0.73 to 193.38) times higher compared to animals from group 1. At days 5–8, BCG-SARS-CoV-2 animals (group 2) showed a relative risk of developing brain lesions of 2 (HE 95%IC=0.88–4.54) and 1.5 (IHC 95% IC=0.60–3.73) times higher compared to animals from group 1.

At 3–4 dpi, group 2 showed mild neuronal and microglial immunoexpression against SARS-CoV-2 in 5 out of 11 cases, while group 1 displayed none in 12 cases. Notably, at 3 dpi, group 2 [2 out of 5 cases; IHC (IS) range=2–6] exhibited oligofocal immunoexpression in the olfactory bulb, orbital cortex, pyriform cortex, olfactory tubercle, the nucleus of the lateral olfactory tract and the medio dorsal thalamic nucleus. At 4 dpi, group 2 (3 out of 6 cases; IS range=6–18), showed more widespread viral immunoexpression with infected neuronal aggregates in the olfactory pathway areas. In addition, infected single neurons began to appear in frontal cortex, as well as periventricular nucleus of the septum/striatum, thalamus, hypothalamus, mesencephalon, pons and spinal cord.

At 5 dpi, both BCG-SARS-CoV-2 (Group 2, 1 out of 1 case; IS range=42) and SARS-CoV-2 groups (Group 1, 1 out of 1 case; IS range=38) exhibited an evident

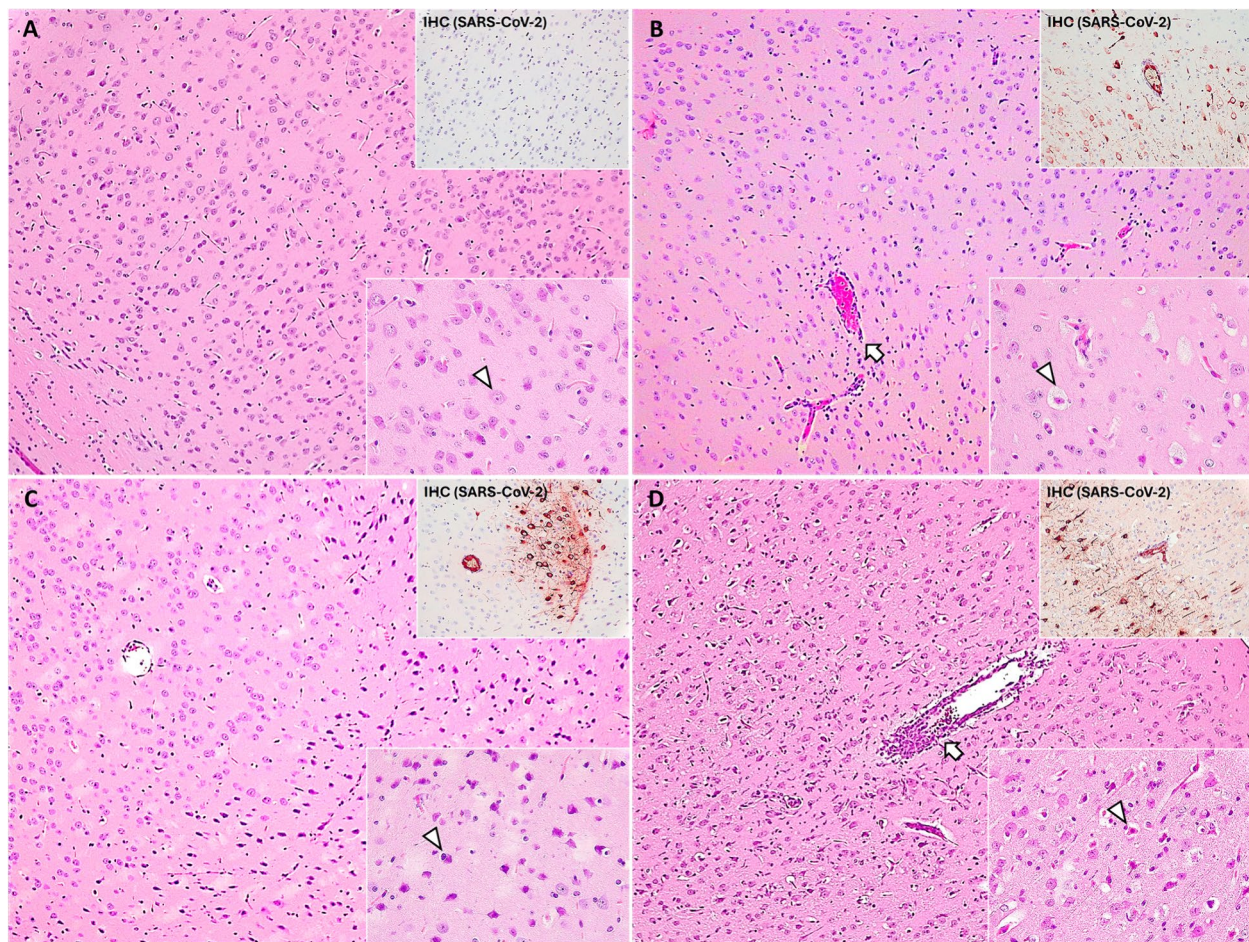


Figure 4 Microscopic brain lesions and viral distribution in the orbital cortex in group 1 (SARS-CoV-2) and group 2 (BCG-SARS-CoV-2) at 3–4 (A, C) and 5–7 dpi (B, D). **A** Absence of lesions with a normal glial cell population number; HE, $\times 10$. Lower right inset: non-damaged neuron (arrowhead); HE, $\times 40$. Upper right inset: absence of SARS-CoV-2 immunoreactivity; IHC, $\times 20$. **B** Mild to moderate perivascular lymphocytic cuffs (arrow); HE, $\times 10$. Lower right inset: moderate number of neurons with cytoplasmic ballooning and shrunken red nuclei (neuronal degeneration—arrowhead); HE, $\times 40$. Upper right inset: neuronal SARS-CoV-2 immunoreactivity in cortical layers IV–V; IHC, $\times 20$. **C** Moderate number of perivascular shrunken neurons. HE, $\times 10$. Lower right inset: shrunken basophilic neurons and activated microglia surrounding the soma (arrowhead); HE, $\times 40$. Upper right inset: perivascular neuronal aggregation with SARS-CoV-2 immunoreactivity; IHC, $\times 20$. **D** Severe perivascular lymphocytic cuffs (arrow) and increased number of glial cell population. HE, $\times 10$. Lower right inset: severe number of neurons with neuronal degeneration and activated microglia surrounding the soma (arrowhead); HE, $\times 40$. Upper right inset: neuronal SARS-CoV-2 immunoreactivity in cortical layers IV–V; IHC, $\times 20$.

increase of viral spreading. Multifocal to coalescent/diffuse neuronal immunoreactivity was observed, noting the onset of hippocampal infection. At 6–7 dpi, BCG-SARS-CoV-2 (Group 2, 5 out of 5 cases; IS range = 37–44) and SARS-CoV-2 (Group 1, 3 out of 3 cases; IS range = 36–44) animals displayed their maximum peak antigen presence. Despite the virus dissemination being highly similar in both groups, there was an apparent reduction in the number of neurons exhibiting positive immunoreactivity in the BCG-SARS-CoV-2 group, potentially attributed to an increase in the number of dead neurons. Cerebellar neurons

showed no infection, but microglial immunoreactivity adjacent to perivascular cuffs was observed in the cerebellar white matter. Animals sacrificed at 8 dpi did not display IHC antigen expression. Overall, a significantly higher total histopathological and IHC score were observed in BCG-SARS-CoV-2 animals (total HS = 1793; total IS = 296) than SARS-CoV-2 animals (total HS = 825; total IS = 158) (Mann–Whitney test HS $p = 0.002$; Mann–Whitney test IS, $p = 0.006$). Additional file 3 shows more detailed information concerning histopathological score results. Detailed histopathological and IHC images comparing both groups are shown in Additional file 4.

Severity of lung lesions was slightly higher in BCG-stimulated SARS-CoV-2 challenged mice

Lungs are one of the most affected organs by SARS-CoV-2 infection, so a histological study was carried out to determine differences between BCG-stimulated and non-stimulated challenged animals. ACE2-expressing alveolar type 2 pneumocytes and goblet cells are the main targets, among others, of SARS-CoV-2 in human lungs [42]. The primary finding in this study was bronchointerstitial pneumonia, characterized by infiltration of mononuclear cells (mainly macrophages and T lymphocytes) and occasional neutrophils around bronchioles and blood vessels. Group 2 exhibited a significantly more moderate pneumonia than group 1 (Mann–Whitney test, $p=0.007$), with this difference being significantly more pronounced at 5–8 dpi (Mann–Whitney test, $p=0.028$) (Figure 5). Animals in group 2 exhibited a significantly higher frequency of inflammatory cell infiltration in the

alveolar interstitium (Mann–Whitney test, $p=0.017$) and pleura (Mann–Whitney test, $p=0.009$), with those inflammatory foci mainly consisting of mononuclear cells (including abundant foamy macrophages).

Vascular and oedematous lesions were frequent, being group 2 the one exhibiting the highest occurrences of vascular thrombosis and perivascular oedema at 3–4 dpi even though observed differences in animals sacrificed in these dpi were not statistically significant (Mann–Whitney test, $p=0.630$; $p=0.551$ respectively). In addition, type II pneumocyte hyperplasia and bronchiolar epithelium hyperplasia were more intense in the group 2, mainly at 5–8 dpi even though no significant differences were detected in these days post-infection (Mann–Whitney test, $p=0.442$; $p=0.083$ respectively). On the other hand, atelectasis was significantly more intense in group 2 at 5–8 dpi (Mann–Whitney test, $p=0.038$). Detailed histopathological images of the

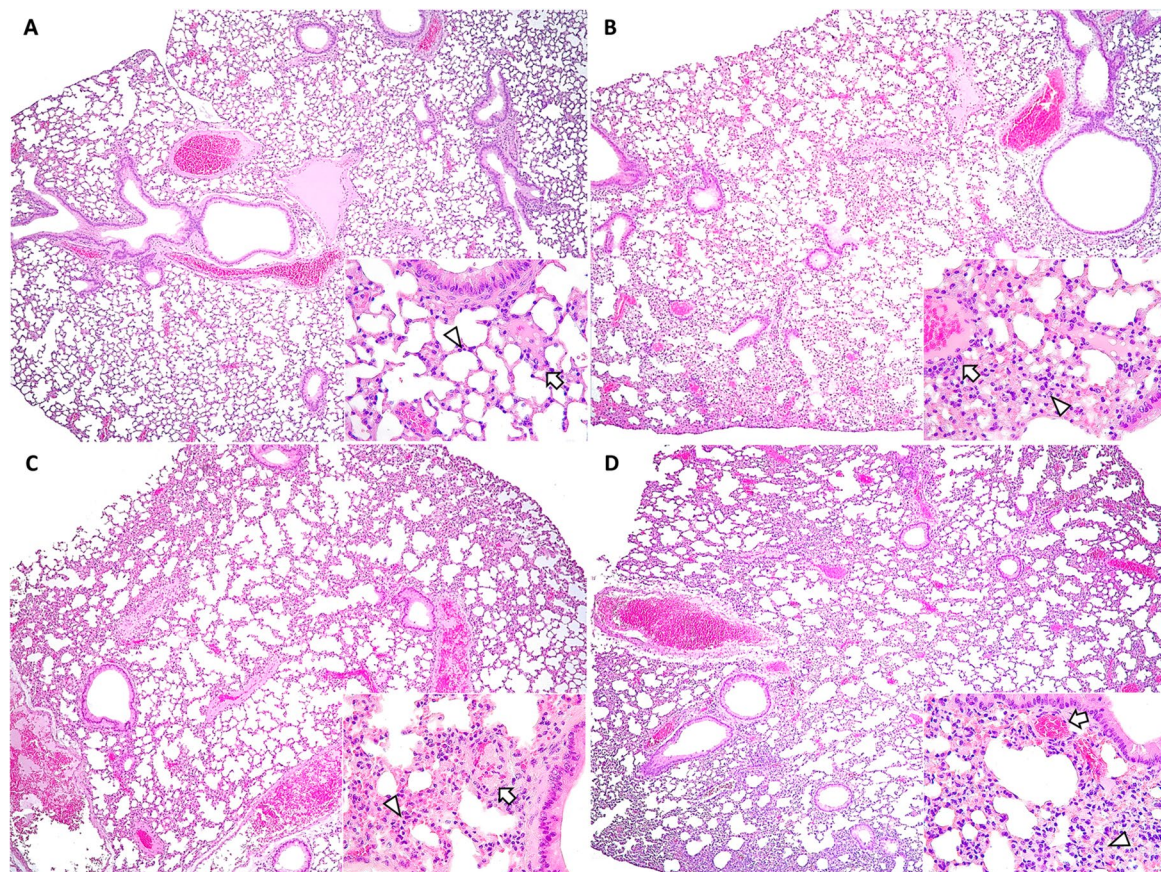


Figure 5 Microscopic lung lesions in mice from: group 1 (SARS-CoV-2) at 3–4 dpi (A) and 5–8 dpi (B); and group 2 (BCG-SARS-CoV-2) at 3–4 dpi (C) and 5–8 dpi (D). **A** Absence of lesions; HE, $\times 10$. Lower right inset: normal alveolar septum thickness (arrowhead) and no perivascular inflammation (arrow); HE, $\times 40$. **B** Mild to moderate and patchy thickening of alveolar septum; HE, $\times 10$. Lower right inset: moderate interstitial pneumonia (arrowhead) and perivascular lymphocytic inflammation (perivascular cuffs—arrow); HE, $\times 40$. **C** Mild to moderate patchy thickening of alveolar septum; HE, $\times 10$. Lower right inset: mild to moderate interstitial pneumonia (arrowhead) and vascular thrombosis (arrow); H&E, $\times 40$. **D** Moderate thickening of alveolar septum thickness; HE, $\times 10$. Lower right inset: moderate interstitial pneumonia (arrowhead) and mild perivascular cuffs (arrow); HE, $\times 40$.

BCG- SARS-CoV-2 group at 5–8 dpi are presented in Additional file 5.

The Additional file 6 shows the immunohistochemical assessment of cellular markers to detect the lymphocytic phenotype and the presence of macrophages in the inflammatory reaction observed in both brain and lungs.

BCG stimulation modified plasma inflammatory and coagulation biomarkers response at different post-immunomodulation days

Variations and abnormalities in plasma inflammatory and coagulation biomarkers have been noted at different stages of the disease in human patients [43]. For this reason, an evaluation of these parameters was carried out to assess if there were any differences between experimental groups 1 and 2. Results for plasma inflammatory and coagulation biomarkers for each animal are shown in Table 4 with median values for experimental groups 1 and 2. These parameters were compared between experimental groups in general and in two different periods post-infection: 3–4 dpi and development of disease (5–8 dpi). There were significant differences in the D-dimer values between both groups, presenting higher values the BCG-SARS-CoV-2 group (Mann–Whitney test, $p=0.019$) (Figure 6, Table 4). In contrast, iNOS values were higher in SARS-CoV-2 animals (group 1) (Figure 6, Table 4) (Mann–Whitney test, $p=0.01$) in general and, comparing both groups at 3–4 dpi (Mann–Whitney test, $p=0.013$) (Figure 6). Animals from BCG-SARS-CoV-2 group showed higher values for TNF- α , compared to animals from group 1 (Mann–Whitney test, $p=0.01$). These significant

differences were also observed on 3–4 dpi ($p=0.022$) (Table 4, Figure 6).

Discussion

Following the COVID-19 pandemic, a question arose about the potential benefits of BCG vaccination in enhancing the immune response against SARS-CoV-2 [15]. Controversial results have emerged from both epidemiological and experimental investigations [26, 30, 34–36, 44]. For this reason, more studies are needed to clarify and test the effect of BCG prior to SARS-CoV-2 infection [27, 45].

In this study, it was investigated whether prior BCG stimulation might affect clinical signs, morbidity, mortality, plasma inflammatory/coagulation biomarkers, and cytokine values following SARS-CoV-2 experimental infection. In addition, viral loads (nasal turbinates/trachea, lung, and brain) by RT-qPCR and histopathology (lung and brain) were assessed. Immunohistochemical analysis was also carried out to confirm invasion and spread of the virus in brain areas. It is important to note that this experimental model is associated with an increased lethality due to SARS-CoV-2 infection and higher neurodissemination compared to humans. In fact, some limitations of this animal model are the risk of ectopic hACE2 expression which changes the cellular tropism of the virus, as well as non-physiological levels of hACE2 expression [46]. Additionally, this model lacks the ability to induce comorbidities as seen in humans [47]. Even K18-hACE2 model does not fully replicate the COVID-19 signs observed in humans, it serves as a valuable model for studying brain invasion

Table 4 Median values and standard deviation for D-dimer, CRP (C-reactive protein), ferritin, iNOS (nitric oxide synthase) as well as for cytokines [interleukin 1 β (IL-1 β), interleukin 1 receptor antagonist (IL-1ra), interleukin 6 (IL-6), tumour necrosis factor alpha (TNF- α), interferon gamma (IFN- γ), and transforming growth factor beta-1 (TGF- β 1)] for group 1 (SARS-CoV-2) and 2 (BCG-SARS-CoV-2) in the moment of the sacrifice

	All			3–4 dpi			Development (5–8 dpi)		
	Group 1	Group 2	<i>p</i> -value	Group 1	Group 2	<i>p</i> -value	Group 1	Group 2	<i>p</i> -value
D-Dimer	27.46 ± 11.29	33.68 ± 47.33	0.019	27.81 ± 7.45	33.68 ± 59.08	0.09	28.90 ± 13.42	57.72 ± 13.75	0.515
C-reactive protein	4974 ± 1869.15	5234 ± 3278.97	0.094	4747 ± 1542.37	4096 ± 827.52	0.621	6073.65 ± 1961.56	7490.39 ± 1795.22	1
Ferritin	1258.20 ± 391.65	1038.48 ± 515.15	0.107	1107.62 ± 301.28	1046.96 ± 688.12	1	1416.33 ± 466.70	1059.17 ± 624.00	0.515
iNOS	49.59 ± 16.62	29.91 ± 14.55	0.01	52.62 ± 15.71	29.40 ± 8.04	0.013	35.26 ± 14.32	25.79 ± 19.87	0.869
IL1- β	8.035 ± 87.19	7.85 ± 3.93	0.821	20.8 ± 13.58	10.7 ± 3.64	0.652	4.23 ± 3.68	6.94 ± 4.52	1
IL-ra	220 ± 149.02	149 ± 79.69	0.165	223 ± 87.68	124 ± 90.63	0.0956	165 ± 265.04	190.5 ± 59.68	1
IL-6	2.32 ± 78.69	3.78 ± 55.98	0.941	2.64 ± 108.05	3.78 ± 7.42	0.943	4.13 ± 14.59	5.46 ± 90.55	1
TNF- α	2.5 ± 102.92	4.55 ± 2.73	0.01	2.34 ± 0.55	3.87 ± 3.01	0.022	3.71 ± 189.53	7.09 ± 1.63	0.515
IFN- γ	0.219 ± 0.90	1.25 ± 8.47	0.096	0.15 ± 0.96	0.38 ± 1.50	0.0956	1.10 ± 0.57	2.86 ± 14.51	0.66
TGF- β 1	4999 ± 4638.84	4010 ± 4247.79	0.941	3345 ± 4847.62	4010 ± 4396.57	0.757	5678.5 ± 4550.38	3822 ± 4001.07	0.515

Statistically significant *p*-values are highlighted in bold. Missing results are due to the limited plasma volume, which did not allow the analysis of all parameters in some animals.

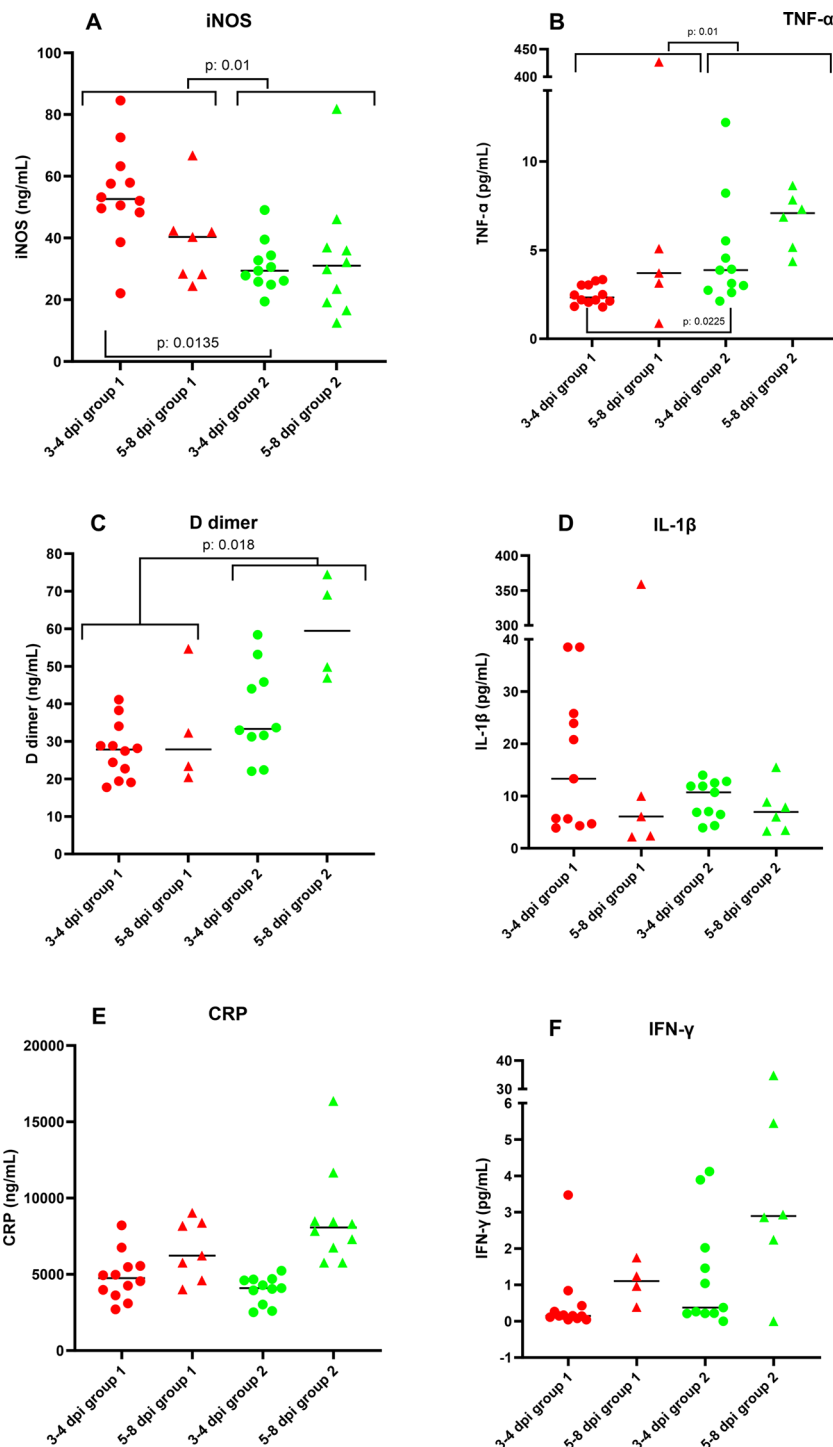


Figure 6 Plot representation of the results obtained for iNOS (A), CRP (C), D-dimer (E) in ng/mL, and the cytokines TNF-α (B), IL1-β (D) and IFN-γ (F) (pg/mL) for each group. These groups are separated in two different subgroups: 3–4 dpi (red dots for group 1 and green dots for group 2) and development of disease (5–8 dpi) (red triangles for group 1 and green triangles for group 2). Horizontal bars represent the median of the values for each group. Missing results are due to the limited plasma volume, which did not allow the analysis of all parameters in some animals.

and dissemination [48]. The experimental model is one of the factors that could lead to differences in BCG effect yet experimental studies in other animal models such as golden Syrian hamster [37], report the IV BCG protection to an even higher dose of SARS-CoV-2 than the one used in this study.

Our results indicate that BCG stimulation did not protect K18-hACE2 mice against SARS-CoV-2 in the assayed conditions; in fact, there was a tendency for increased severity, in contrast to previous studies [34, 35, 37]. In group 1 (SARS-CoV-2), only 4 out of 10 mice presented clinical signs, while in the BCG-SARS-CoV-2 mice (group 2), 6 out of 10 showed signs of illness. Reduced activity and weight loss were the most common clinical signs observed in sick mice, regardless of their experimental group, as previously observed [49]. This contrasts with the study by Hilligan et al. [30], where BCG-SARS-CoV-2 animals showed no clinical signs, and the study by Kaufmann et al. [35], in which no differences were observed between the two experimental groups.

Regarding the presence of SARS-CoV-2 in brain tissue, the number of PCR-positive samples was significantly higher in BCG-SARS-CoV-2 challenged mice. The maximum peak was observed at 6–7 dpi, which is in accordance with Carossino et al. [41] and differs from Hilligan et al. [30], a study in which the highest virus levels were observed at 5 dpi, but they only measured viral loads levels at 3 and 5 dpi. In this study, elevated viral loads as well as higher neuroinvasion was detected in the BCG-SARS-CoV-2 group when comparing to the SARS-CoV-2 group, with a significant difference observed at early stages (3–4 dpi). These results contrast with other comparative studies between these two experimental groups in which the same challenge dose was used for infection and no significant differences were observed [30].

Neuroinvasion, the primary cause of SARS-CoV-2 lethality in K18-hACE2 mice [41], has been well-documented in both experimental mouse models [31, 32, 48] and humans [50, 51]. This study further enhances our understanding of SARS-CoV-2 neuroinvasion and pathogenic mechanisms in this experimental model.

The exact pathways of virus entry into neuronal tissues remain controversial. One plausible hypothesis is the olfactory pathway, as SARS-CoV-2 antigens and RNA have been detected in sustentacular cells and Bowman glands [4]. Indeed, in k18-hACE mice ACE2 receptors are notably elevated in the olfactory bulb and in pericytes and endothelial cells [52]. It has also been demonstrated that SARS-CoV-2 is able to infect and cross through microvascular endothelial cells (BMECs), present in the BBB (Blood Brain Barrier) [53]. However, other molecules, like neuropilin-1 (NRP1), especially

in olfactory neuroepithelial cells, may also facilitate the viral entry [54]. The present study chronologically examined the most affected areas by SARS-CoV-2 in CNS (central nervous system), revealing virus presence in olfactory-related regions (olfactory bulb, olfactory tubercle, nucleus of the lateral olfactory tract), thalamus, and orbital cortex at 3 dpi. The presence of SARS-CoV-2 in the olfactory bulb has also been appreciated in other studies in k18-hACE2 [32, 33] or humans [55], though the contrary has also been stated [56, 57]. The presence of the virus in this location could explain the altered olfactory reception in k18-hACE2 mice [33], as this information is sent from the olfactory bulb to the orbitofrontal cortex via the dorsal medial nucleus of the thalamus [58], through neuron-to-neuron axonal transport [59]. However, this hypothesis is less likely in humans, as it is suggested that anosmia is primarily caused by a disruption in the olfactory epithelium, where SARS-CoV-2 infects non-neuronal cell types, leading to tissue damage and inflammation [60]. From 4 dpi onwards, infected neuronal aggregations suggest trans-synaptic viral spread between neurons [32], often adjacent to affected blood vessels. In BCG-SARS-CoV-2 mice, at 4 dpi, infection of the subarachnoid space from the olfactory bulb resulted in perivascular meningitis. This space contains crucial large brain blood vessels, potentially affecting BBB permeability. By 5 dpi, high immunoexpression was observed in ventricular areas, vulnerable regions to BBB disruption, alongside reduced immunoexpression in the olfactory bulb or pyriform cortex. In later stages (5–7 dpi), multifocal to diffuse infected areas closely related to vascular and ventricular structures were observed. These findings suggest that after the initial entry via the olfactory pathway, the BBB is altered, promoting hematogenous dissemination, with a possible role of leukocytes carrying SARS-CoV-2 in this process [32].

SARS-CoV-2 was only found in vessels and microglia in the white matter near the pons, raising questions about whether the absence of viral particles found in cerebellar neurons in this study would be due to receptor scarcity [32] or animals dying before virus reaches grey matter area of the cerebellum. Further studies would be necessary to elucidate the viral chronology and presence in these structures.

BCG-SARS-CoV-2 mice presented more severe brain lesions than SARS-CoV-2 animals, consisting of increased glial cells (microglia mainly), T lymphocyte infiltration, and neurodegeneration. In cases of CNS insult, peripheral proinflammatory cytokines such as IL-1, TNF- α , IL-6, IL-12 as well as thrombin, fibrinogen and plasmin concentrations elevate after SARS-CoV-2 infection [61]. This event can cause hypoxia [61],

microgliosis and astrogliosis [62] followed by a BBB break down allowing SARS-CoV-2 entrance in the CNS [61, 63], which could be potentially exacerbated in BCG-SARS-CoV-2 animals. The TNF- α , one of the major mediators of the neuroinflammation associated with neurodegeneration, was increased in plasma in BCG-SARS-CoV-2 group probably because of an enhanced Th1 response in these animals [64, 65]. Higher D-dimer levels were also observed in this group, linked to the risk of venous thromboembolism [66]. Similarly, vascular thrombosis was observed in lungs with a slight increase in BCG-SARS-CoV-2 animals. Significantly higher levels of iNOS were observed in the SARS-CoV-2 mice (group 1), which could have possibly played a role in the lower thrombosis events encountered in these animals [67, 68].

The respiratory pathway plays a pivotal role in the SARS-CoV-2 infection process, which is the main reason for its rapid transmission [69]. In our study, both experimental groups (BCG-SARS-CoV-2 and SARS-CoV-2) exhibited similar viral loads in the lungs in contrast with other studies [34, 37] that used different experimental model, dose or strain respectively, obtaining lower viral loads in lungs on BCG inoculated animals. In our study, inflammatory infiltrates were mainly composed of macrophages and lymphocytes, a phenomenon observed by other researchers [42]. Nevertheless, inflammatory lesions were slightly increased in BCG-SARS-CoV-2 mice (group 2) compared to SARS-CoV-2 group. These results contrast with previous studies suggesting that BCG curtails SARS-CoV-2 induced disease severity and lung inflammation [30, 34].

Given all the aforementioned and the discrepancies of this study compared to others that have been carried out to assess the efficacy of BCG against SARS-CoV-2 [30, 34, 37], we posit the possibility that these differences may be attributed to the SARS-CoV-2 variant, the infection dose and the experimental model as already mentioned, as well as the different BCG strain, route and time of BCG administration. Concerning the BCG strain, variations in protective effects against tuberculosis have been demonstrated [70], which could impact the ability to induce protection against unrelated pathogens [71]. In our study, we used the Danish CCUG 27863 strain, while previous studies utilized the Tokyo [34], Pasteur [72], and TICE [35] strains. At this point, it should be considered that previous experiments of our group have demonstrated that animals immunized with the Danish CCUG 27863 strain did not show any vascular or inflammatory changes in brain tissue (data not shown). Thus, we discard that neurological lesions are due to the direct action of BCG. The route of BCG administration may also be relevant, as some studies have assessed the

route's importance in inducing trained immunity [73]. Previous studies in k18-hACE2 mice model used the subcutaneous route for BCG administration and this route failed to protect against SARS-CoV-2 [30, 34, 35]. In fact, BCG intravenous inoculation has been suggested as the only route capable of inducing trained immunity [30, 34] against SARS-CoV-2. However, in our study, even with BCG intravenous inoculation, protection against SARS-CoV-2 was not achieved. SARS-CoV-2 variants have been associated with different neuroinvasive patterns in K18-hACE2 mice [74], potentially explaining different levels of BCG-mediated trained immunity protection against this virus in other studies challenging with different variants [34, 35, 72].

In conclusion, the broad benefits of trained immunity induced by BCG enhancing the host's immune response against heterologous pathogens [75] and even enhance antitumour immune response [76] have been widely demonstrated. Nevertheless, potential detrimental impact on inflammatory disease has also been suggested in mice [77]. Our results suggest that the dysregulation of innate immune system during SARS-CoV-2 infection [27] could be exacerbated in BCG-stimulated-challenged animals which may lead to a potential harmful impact on the neurological system. This research might constitute a starting point for discussions on the risk of potential adverse outcomes due to the non-specific effects of BCG vaccination.

Supplementary Information

The online version contains supplementary material available at <https://doi.org/10.1186/s13567-024-01325-7>.

Additional file 1. Representation of clinical scores of infected animals at the day of sacrifice and viral loads (brain, lung, trachea/nasal turbinates) from both groups. *The clinical score from this animal could not be recorded because it was found dead at 7 dpi. **These scores correspond to the day on which the animals were euthanized which coincided with the day of the highest clinical score.

Additional file 2. Detailed histological score of the animals from both groups for the different brain sections. Sections analysed are: olfactory bulb, pyriform cortex, septum-striatum, cerebral cortex, hippocampus, thalamus, hypothalamus, caudal mesencephalon, pons, cerebellum, and spinal cord scoring each lesion from 0 to 5.

Additional file 3. Detailed neuronal immunoeexpression score of the animals from both groups for the different brain sections. Immunoeexpression was scored from 0 to 5 according to their degree of extension, based on the proportion of affected neurons.

Additional file 4. Brain lesions and SARS-CoV-2 IHC observed in SARS-CoV-2 (A, C, E, G, I, K, M, O) and BCG-SARS-CoV-2 (B, D, F, H, J, L, N, P) at 7 dpi. These analyses were performed in specific areas like orbital cerebral cortex (precentral area) (A, B), septum (C, D), pyriform cortex (E, F), olfactory tubercle (G, H), cerebral cortex (postcentral area) (I, J), thalamus (K, L), mesencephalon (M, N) and pons (O, P). Histopathological study revealed more severe lesions in the BCG-stimulated animals, highlighting perivascular lymphocytic cuffings, increase in glial cell population (mainly microglia) and neuronal degeneration, characterized by red neurons and cytoplasmic ballooning;

H&E, 10x. IHC of SARS-CoV-2 (insets) revealed a higher number of infected neurons in non-stimulated group at 7 dpi; IHC, 20x.

Additional file 5. Main microscopic changes observed in the lungs of BCG-SARS-CoV-2 mice at 5–8 days post SARS-COV-2 infection. (A) Perivascular and peribronchiolar mononuclear cell infiltration, hyperplasia of the bronchiolar epithelium and foci of pleuritis; H&E, 10x. (B) Vascular thrombosis; H&E, 20x. (C) Abundant foamy macrophages in the alveolar interstitium; H&E, 40x. (D) Desquamative alveolitis; H&E, 40x.

Additional file 6. IHC evaluation (CD3, PAX5, Iba-1) in brain (A, B, C) and lungs (D, E, F) of BCG-SARS-CoV-2 mice at 5–8 days post-infection. (A) CD3⁺ T cells immunoeexpression in lymphocytic perivascular cuffings (arrowhead); anti-CD3, 40x. (B) No presence of PAX5⁺ B cells immunoeexpression in lymphocytic perivascular cuffings; anti-PAX5, 40x. (arrowhead). (C) Iba-1⁺ microglial cells immunoeexpression surrounding lymphocytic perivascular cuffings (arrowhead); anti-Iba-1, 20x. (D) CD3⁺ T cells immunoeexpression in lymphocytic perivascular cuffings and alveolar interstitium (arrowhead); anti-CD3, 40x. (E) Minimal presence of PAX5⁺ B cells immunoeexpression in lymphocytic perivascular cuffings; anti-PAX5, 40x. (arrowhead). (F) Iba-1⁺ macrophages immunoeexpression in pulmonar interstitium (arrowhead); anti-Iba-1, 20x. Inset: Iba-1⁺ foamy macrophages immunoeexpression in alveolar interstitium; anti-Iba-1, 40x.

Acknowledgements

Authors would like to thank María del Carmen Jimenez, Deborah López and Rocío Sánchez for their excellent technical support, as well as Andrea Pérez and Kiara Acurio for their invaluable help. Also, we would like to thank Luis Enjuanes for kindly providing us the SARS-CoV-2 virus, the ISCIII for their support in the cytokine analysis and MYCOTRAINING group for their support in the development of the present study.

Authors' contributions

RJ, MD, and LD worked in the conception of the study. LD directed the research and TGS (animal model), JF (proteomic study), CG, MD and LD designed the study. The main acquisition of data was carried out by LSM (general), NP (pathological study), FC (hematological analysis), BC (pathological study), SBA (viral analysis), MDF (viral analysis), A Buendía (BCG analysis), IM (immunological study) and MD (immunological study) and interpretation of data by LSM (general), NP (general), TGS (statistical analysis), MPS (general), FC (general), BC (pathological study), MAR (pathological and immunological study), A Balseiro (pathological study), ARB (pathological study). Original draft was written by LSM, NP, TGS, MPS, FC and reviewed and edited by BC, SBA, MDF, IM, VB, MAR, JF, RJ, JG, A Balseiro, CG, ARB, MD, and LD. Finally, the funding acquisition was obtained by MPS and LD. All authors read and approved the final manuscript.

Funding

This research was partially funded by a REACT-European Union grant from the Comunidad de Madrid to the ANTICIPA project of Complutense University of Madrid (reference PR38/21) and partially funded by PID2020-112966RB-I00 financed by MCIN/AEI/10.13039/501100011033. The funders had no role in study design, data collection and analysis, preparation of the manuscript or decision to publish.

Availability of data and materials

All data generated or analysed during this study are included in this published article [and its supplementary information files].

Declarations

Ethics approval and consent to participate

Animal care and procedures were performed by following the guidelines of good experimental practices according to Directive 2010/63/EU of the European Parliament and of the Council of 22 September 2010 on the protection of animals used for scientific purposes (amended by the Regulation (EU) 2019/1010) and Spanish laws (RD 53/2013). The protocol was approved by the Community of Madrid Ethics Committee (reference PROEX 180.2/22).

Competing interests

The authors declare that they have no competing interests.

Author details

¹VISAVET Health Surveillance Centre, Complutense University of Madrid, 28040 Madrid, Spain. ²Department of Animal Health, Faculty of Veterinary Medicine, Complutense University of Madrid, 28040 Madrid, Spain. ³Department of Animal Production, Faculty of Veterinary Medicine, Complutense University of Madrid, 28040 Madrid, Spain. ⁴Unidad de Inmunología Microbiana, Centro Nacional de Microbiología, Instituto de Salud Carlos III, Carretera Pozuelo-Majadahonda km 2, Majadahonda, 28220 Madrid, Spain. ⁵Departamento de Anatomía y Anatomía Patológica Comparadas y Toxicología, Grupo de Investigación en Sanidad Animal y Zoonosis (GISAZ), UIC Zoonosis y Enfermedades Emergentes (ENZOEM), Universidad de Córdoba, Córdoba, Spain. ⁶SaBio Instituto de Investigación en Recursos Cinegéticos, Ciudad Real, Spain. ⁷Department of Veterinary Pathobiology, Center for Veterinary Health Sciences, Oklahoma State University, Stillwater, OK, USA. ⁸Animal Health Department, NEIKER-Basque Institute for Agricultural Research and Development, Basque Research and Technology Alliance (BRTA), 48160 Derio, Bizkaia, Spain. ⁹Departamento de Sanidad Animal, Facultad de Veterinaria, Universidad de León, 24071 León, Spain. ¹⁰Department of Internal Medicine and Animal Surgery, Faculty of Veterinary Medicine, Complutense University of Madrid, 28040 Madrid, Spain. ¹¹Real Academia de Doctores de España, C. de San Bernardo, 49, 28015 Madrid, Spain.

Received: 17 November 2023 Accepted: 27 April 2024

Published online: 31 May 2024

References

- Organization WH (2023) WHO health emergency dashboard [on line]. <https://covid19.who.int>
- Mao L, Jin H, Wang M, Hu Y, Chen S, HeQ CJ, Hong C, Zhou Y, Wang D, Miao X, Li Y, Hu B (2020) Neurologic manifestations of hospitalized patients with coronavirus disease 2019 in Wuhan, China. *JAMA Neuro* 77:683–690
- Shen WB, Elahi M, Logue J, Yang P, Baracco L, Reece EA, Wang B, Li L, Blanchard TG, Han Z, Rissman RA, Frieman MB, Yang P (2022) SARS-CoV-2 invades cognitive centers of the brain and induces Alzheimer's-like neuropathology. *BioRxiv*. <https://doi.org/10.1101/2022.01.31.478476>
- Bauer L, Laksono BM, de Vrij FMS, Kushner SA, Harschnitz O, van Riel D (2022) The neuroinvasiveness, neurotropism, and neurovirulence of SARS-CoV-2. *Trends Neurosci* 45:358–368
- Wang Q, Davis PB, Gurney ME, Xu R (2021) COVID-19 and dementia: analyses of risk, disparity, and outcomes from electronic health records in the US. *Alzheimers Dement* 17:1297–1306
- Shirbhate E, Pandey J, Patel VK, Kamal M, Jawaid T, Gorain B, Kesharwani P, Rajak H (2021) Understanding the role of ACE-2 receptor in pathogenesis of COVID-19 disease: a potential approach for therapeutic intervention. *Pharmacol Rep* 73:1539–1550
- Pastrian-Soto G (2020) Presence and expression of ACE2 receptor (target of SARS-CoV-2) in human tissues and oral cavity. Possible routes infection in oral organs. *Int J Odontostomat* 14:501–507 (in Spanish)
- Hamming I, Timens W, Bulthuis ML, Lely AT, Navis G, van Goor H (2004) Tissue distribution of ACE2 protein, the functional receptor for SARS coronavirus. A first step in understanding SARS pathogenesis. *J Pathol* 203:631–637
- Piras M, Cau F, Manchia M, Paribello P, Saba L, Suri JS, Faa G, Pichiri G, Cerrone G, Scano A, Orru G, La Nasa G, Coghe F, Castagnola M, Fanni D, Gerosa C (2022) Strong ACE-2 expression in the choroidal vessels: do high choroid plexuses serve as a gateway for SARS-CoV-2 infection on the human brain? *Eur Rev Med Pharmacol Sci* 26:3025–3029
- Pellegrini L, Albecka A, Mallery DL, Kellner MJ, Paul D, Carter AP, James LC, Lancaster MA (2020) SARS-CoV-2 infects the brain choroid plexus and disrupts the blood-CSF barrier in human brain organoids. *Cell Stem Cell* 27:951–961.e5
- Rahman S, Montero MTV, Rowe K, Kirton R, Kunik F (2021) Epidemiology, pathogenesis, clinical presentations, diagnosis and treatment of COVID-19: a review of current evidence. *Expert Rev Clin Pharmacol* 14:601–621

12. Jin JM, Bai P, He W, Wu F, Liu XF, Han DM, Liu S, Yang JK (2020) Gender differences in patients with COVID-19: focus on severity and mortality. *Front Public Health* 8:152
13. Gamble A, Pham Q, Goyal S, Cafazzo JA (2020) The challenges of COVID-19 for people living with diabetes: considerations for digital health. *JMIR Diabetes* 5:e19581
14. Gérard C, Maggipinto G, Minon JM (2020) COVID-19 and ABO blood group: another viewpoint. *Br J Haematol* 190:e93–e94
15. Gursel M, Gursel I (2020) Is global BCG vaccination-induced trained immunity relevant to the progression of SARS-CoV-2 pandemic? *Allergy* 75:1815–1819
16. Yamazaki-Nakashimada MA, Unzueta A, Berenise Gamez-Gonzalez L, Gonzalez-Saldana N, Sorensen RU (2020) BCG: a vaccine with multiple faces. *Hum Vaccin Immunother* 16:1841–1850
17. Gomes RR, Antunes DE, Dos Santos DF, Sabino EFP, Oliveira DB, Goulart IMB (2019) BCG vaccine and leprosy household contacts: protective effect and probability of becoming sick during follow-up. *Vaccine* 37:6510–6517
18. Morra ME, Kien ND, Elmaraezy A, Abdelaziz OAM, Elsayed AL, Halhouli O, Montasr AM, Vu TL, Ho C, Foly AS, Phi AP, Abdullah WM, Mikhail M, Milne E, Hirayama K, Huy NT (2017) Early vaccination protects against childhood leukemia: a systematic review and meta-analysis. *Sci Rep* 7:15986
19. Usher NT, Chang S, Howard RS, Martinez A, Harrison LH, Santosham M, Aronson NE (2019) Association of BCG vaccination in childhood with subsequent cancer diagnoses: a 60-year follow-up of a clinical trial. *JAMA Netw Open* 2:e1912014
20. van Puffelen JH, Keating ST, Oosterwijk E, van der Heijden AG, Netea MG, Joosten LAB, Vermeulen SH (2020) Trained immunity as a molecular mechanism for BCG immunotherapy in bladder cancer. *Nat Rev Urol* 17:513–525
21. Kleinnijenhuis J, Quintin J, Preijers F, Joosten LA, Iffrim DC, Saeed S, Jacobs C, van Loenhout J, de Jong D, Stunnenberg HG, Xavier RJ, van der Meer JW, van Crevel R, Netea MG (2012) Bacille Calmette–Guerin induces NOD2-dependent nonspecific protection from reinfection via epigenetic reprogramming of monocytes. *Proc Natl Acad Sci USA* 109:17537–17542
22. Covian C, Retamal-Diaz A, Bueno SM, Kalgiris AM (2020) Could BCG vaccination induce protective trained immunity for SARS-CoV-2? *Front Immunol* 11:970
23. O'Neill LAJ, Netea MG (2020) BCG-induced trained immunity: can it offer protection against COVID-19? *Nat Rev Immunol* 20:335–337
24. Netea MG, van der Meer JW, van Crevel R (2021) BCG vaccination in health care providers and the protection against COVID-19. *J Clin Invest* 131:e145545
25. de la Fuente J, Armas O, Sánchez-Rodríguez L, Gortázar C, Lukashev AN, COVID-BCG Collaborative Working Group (2021) Citizen science initiative points at childhood BCG vaccination as a risk factor for COVID-19. *Transbound Emerg Dis* 68:3114–3119
26. Claus J, Ten Doesschate T, Gumbs C, van Werkhoven CH, van der Vaart TW, Janssen AB, Smits G, van Binnendijk R, van der Klis F, van Baarle D, Paganelli FL, Leavis H, Verhagen LM, Joosten SA, Bonten MJM, Netea MG, van de Wijkert J, Group BC-CS (2023) BCG vaccination of health care workers does not reduce SARS-CoV-2 infections nor infection severity or duration: a randomized placebo-controlled trial. *MBio* 14:e0035623
27. Kaur G, Singh S, Nanda S, Zafar MA, Malik JA, Arshi MU, Lamba T, Agrewala JN (2022) Fiction and facts about BCG imparting trained immunity against COVID-19. *Vaccines* 10:1006
28. Moreau GB, Burgess SL, Sturek JM, Donlan AN, Petri WA, Mann BJ (2020) Evaluation of K18-hACE2 mice as a model of SARS-CoV-2 infection. *Am J Trop Med Hyg* 103:1215–1219
29. Munoz-Fontela C, Dowling WE, Funnell SGP, Gsell PS, Riveros-Balta AX, Albrecht RA, Andersen H, Baric RS, Carroll MW, Cavaleri M, Qin C, Crozier I, Dallmeier K, de Waal L, de Wit E, Delang L, Dohm E, Duprex WP, Falzarano D, Finch CL, Frieman MB, Graham BS, Gralinski LE, Guilfoyle K, Haagmans BL, Hamilton GA, Hartman AL, Herfst S, Kaptein SJF, Klimstra WB et al (2020) Animal models for COVID-19. *Nature* 586:509–515
30. Hilligan KL, Namasivayam S, Clancy CS, O'Mard D, Oland SD, Robertson SJ, Baker PJ, Castro E, Garza NL, Lafont BAP, Johnson R, Ronchese F, Mayer-Barber KD, Best SM, Sher A (2022) Intravenous administration of BCG protects mice against lethal SARS-CoV-2 challenge. *J Exp Med* 219:e20211862
31. Song E, Zhang C, Israelow B, Lu-Culligan A, Prado AV, Skriabine S, Lu P, Weizman OE, Liu F, Dai Y, Szigeti-Buck K, Yasumoto Y, Wang G, Castaldi C, Heltke J, Ng E, Wheeler J, Alfajaro MM, Levavasseur E, Fontes B, Ravindra NG, Van Dijk D, Mane S, Gunel M, Ring A, Kazmi SAJ, Zhang K, Wilen CB, Horvath TL, Plu I, Haik S, Thomas JL, Louvi A, Farhadian SF, Huttner A, Seilhean D, Renier N, Bilguvar K, Iwasaki A (2021) Neuroinvasion of SARS-CoV-2 in human and mouse brain. *J Exp Med* 218:e20202135
32. Vidal E, Lopez-Figueroa C, Rodon J, Perez M, Brustolin M, Cantero G, Guallar V, Izquierdo-Useros N, Carrillo J, Blanco J, Clotet B, Vergara-Alert J, Segales J (2022) Chronological brain lesions after SARS-CoV-2 infection in hACE2-transgenic mice. *Vet Pathol* 59:613–626
33. Zheng J, Wong LR, Li K, Verma AK, Ortiz ME, Holford-Lenane C, Leidinger MR, Knudson CM, Meyerholz DK, McCray PB Jr, Perlman S (2021) COVID-19 treatments and pathogenesis including anosmia in K18-hACE2 mice. *Nature* 589:603–607
34. Zhang BZ, Shuai H, Gong HR, Hu JC, Yan B, Yuen TT, Hu YF, Yoon C, Wang XL, Hou Y, Lin X, Huang X, Li R, Au-Yeung YM, Li W, Hu B, Chai Y, Yue M, Cai JP, Ling GS, Hung IF, Yuen KY, Chan JF, Huang JD, Chu H (2022) Bacillus Calmette–Guerin-induced trained immunity protects against SARS-CoV-2 challenge in K18-hACE2 mice. *JCI Insight* 7:e157393
35. Kaufmann E, Khan N, Tran KA, Ulndreaj A, Pernet E, Fontes G, Lupien A, Desmeules P, McIntosh F, Abow A, Moorlag S, Debisarun P, Mossman K, Banerjee A, Karo-Atar D, Sadeghi M, Mubareka S, Vinh DC, King IL, Robbins CS, Behr MA, Netea MG, Joubert P, Divangahi M (2022) BCG vaccination provides protection against IAV but not SARS-CoV-2. *Cell Rep* 38:110502
36. Hildebrand RE, Chandrasekar SS, Riel M, Touray BJB, Aschenbroich SA, Talaat AM (2022) Superinfection with SARS-CoV-2 has deleterious effects on *Mycobacterium bovis* BCG immunity and promotes dissemination of *Mycobacterium tuberculosis*. *Microbiol Spectr* 10:e0307522
37. Singh AK, Wang R, Lombardo KA, Praharaj M, Bullen CK, Um P, Gupta M, Srikrishna G, Davis S, Komm O, Illei PB, Ordóñez AA, Bahr M, Huang J, Gupta A, Psoter KJ, Creisher PS, Li M, Pekosz A, Klein SL, Jain SK, Bivalacqua TJ, Yegnasubramanian S, Bishai WR (2023) Intravenous BCG vaccination reduces SARS-CoV-2 severity and promotes extensive reprogramming of lung immune cells. *iScience* 26:107733
38. Weinberg MS, Zafar A, Magdamo C, Chung SY, Chou WH, Nayan M, Deodhar M, Frenzl DM, Feldman AS, Faustman DL, Arnold SE, Vakulenko-Lagun B, Das S (2023) Association of BCG vaccine treatment with death and dementia in patients with non-muscle-invasive bladder cancer. *JAMA Netw Open* 6:e2314336
39. Baczenas JJ, Andersen H, Rashid S, Yarmosh D, Puthuveetil N, Parker M, Bradford R, Florence C, Stemple KJ, Lewis MG, O'Connor SL (2021) Propagation of SARS-CoV-2 in Calu-3 cells to eliminate mutations in the furin cleavage site of spike. *Viruses* 13:2434
40. Keith BJ, Franklin PG (2001) The mouse brain in stereotaxic coordinates. Academic Press, San Diego
41. Carossino M, Kenney D, O'Connell AK, Montanaro P, Tseng AE, Gertje HP, Grosz KA, Ericsson M, Huber BR, Kurnick SA, Subramaniam S, Kirkland TA, Walker JR, Francis KP, Klose AD, Paragas N, Bosmann M, Saeed M, Balasuriya UBR, Douam F, Crossland NA (2022) Fatal neurodissemination and SARS-CoV-2 tropism in K18-hACE2 mice is only partially dependent on hACE2 expression. *Viruses* 14:535
42. Kim SH, Kim J, Jang JY, Noh H, Park J, Jeong H, Jeon D, Uhm C, Oh H, Cho K, Jeon Y, On D, Yoon S, Lim SY, Kim SP, Lee YW, Jang HJ, Park IH, Oh J, Seo JS, Kim JJ, Seok SH, Lee YJ, Hong SM, An SH, Kim SY, Kim YB, Hwang JY, Lee HJ, Kim HB, et al. (2022) Mouse models of lung-specific SARS-CoV-2 infection with moderate pathological traits. *Front Immunol* 13:1055811
43. Guan WJ, Ni ZY, Hu Y, Liang WH, Ou CQ, He JX, Liu L, Shan H, Lei CL, Hui DSC, Du B, Li LJ, Zeng G, Yuen KY, Chen RC, Tang CL, Wang T, Chen PY, Xiang J, Li SY, Wang JL, Liang ZJ, Peng YX, Wei L, Liu Y, Hu YH, Peng P, Wang JM, Liu JY, Chen Z, et al. (2020) Clinical characteristics of coronavirus disease 2019 in China. *N Engl J Med* 382:1708–1720
44. Ebina-Shibuya R, Horita N, Namkoong H, Kaneko T (2020) Current national policies for infant universal bacille Calmette–Guerin vaccination were associated with lower mortality from coronavirus disease 2019. *Clin Exp Vaccine Res* 9:179–182
45. Chen J, Gao L, Wu X, Fan Y, Liu M, Peng L, Song J, Li B, Liu A, Bao F (2023) BCG-induced trained immunity: history, mechanisms and potential applications. *J Transl Med* 21:106

46. Winkler ES, Bailey AL, Kafai NM, Nair S, McCune BT, Yu J, Fox JM, Chen RE, Earnest JT, Keeler SP, Ritter JH, Kang LI, Dort S, Robichaud A, Head R, Holtzman MJ, Diamond MS (2020) SARS-CoV-2 infection of human ACE2-transgenic mice causes severe lung inflammation and impaired function. *Nat Immunol* 21:1327–1335
47. Ejaz H, Alsrhani A, Zafar A, Javed H, Junaid K, Abdalla AE, Abosalif KOA, Ahmed Z, Younas S (2020) COVID-19 and comorbidities: deleterious impact on infected patients. *J Infect Public Health* 13:1833–1839
48. Seehusen F, Clark JJ, Sharma P, Bentley EG, Kirby A, Subramaniam K, Wunderlin-Giuliani S, Hughes GL, Patterson EI, Michael BD, Owen A, Hiscox JA, Stewart JP, Kipar A (2022) Neuroinvasion and neurotropism by SARS-CoV-2 variants in the K18-hACE2 mouse. *Viruses* 14:1020
49. Kumari P, Rothan HA, Natekar JP, Stone S, Pathak H, Strate PG, Arora K, Brinton MA, Kumar M (2021) Neuroinvasion and encephalitis following intranasal inoculation of SARS-CoV-2 in K18-hACE2 mice. *Viruses* 13:132
50. Hanley B, Naresh KN, Roufosse C, Nicholson AG, Weir J, Cooke GS, Thursz M, Manousou P, Corbett R, Goldin R, Al-Sarraj S, Abdolrasouli A, Swann OC, Bailion L, Penn R, Barclay WS, Viola P, Osborn M (2020) Histopathological findings and viral tropism in UK patients with severe fatal COVID-19: a post-mortem study. *Lancet Microbe* 1:e245–e253
51. Kantonen J, Mahzabin S, Mayranpaa MI, Tynnenen O, Paetau A, Andersson N, Sajantila A, Vapalahti O, Carpen O, Kekalainen E, Kantele A, Myllykangas L (2020) Neuropathologic features of four autopsied COVID-19 patients. *Brain Pathol* 30:1012–1016
52. Chen R, Wang K, Yu J, Howard D, French L, Chen Z, Wen C, Xu Z (2020) The spatial and cell-type distribution of SARS-CoV-2 receptor ACE2 in the human and mouse brains. *Front Neurol* 11:573095
53. Zhang L, Zhou L, Bao L, Liu J, Zhu H, Lv Q, Liu R, Chen W, Tong W, Wei Q, Xu Y, Deng W, Gao H, Xue J, Song Z, Yu P, Han Y, Zhang Y, Sun X, Yu X, Qin C (2021) SARS-CoV-2 crosses the blood–brain barrier accompanied with basement membrane disruption without tight junctions alteration. *Signal Transduct Target Ther* 6:337
54. Cantuti-Castelvetri L, Ojha R, Pedro LD, Djannatani M, Franz J, Kuivanen S, van der Meer F, Kallio K, Kaya T, Anastasina M, Smura T, Levanov L, Szirovicza L, Tobi A, Kallio-Kokko H, Osterlund P, Joensuu M, Meunier FA, Butcher SJ, Winkler MS, Mollenhauer B, Helenius A, Gokke O, Teesalu T, Hepojoki J, Vapalahti O, Stadelmann C, Balistreri G, Simons M (2020) Neuropilin-1 facilitates SARS-CoV-2 cell entry and infectivity. *Science* 370:856–860
55. Klingenstein M, Klingenstein S, Neckel PH, Mack AF, Wagner AP, Kleger A, Liebau S, Milazzo A (2020) Evidence of SARS-CoV2 entry protein ACE2 in the human nose and olfactory bulb. *Cells Tissues Organs* 209:155–164
56. Khan M, Clijsters M, Choi S, Backaert W, Claerhout M, Couvreur F, Van Breda L, Bourgeois F, Speleman K, Klein S, Van Laethem J, Verstappen G, Dereli AS, Yoo SJ, Zhou H, Dan Do TN, Jochmans D, Laenen L, Debaveye Y, De Munter P, Gunst J, Jorissen M, Lagrou K, Meersseman P, Neyts J, Thal DR, Topsakal V, Vandenbrielle C, Wauters J, Mombaerts P, Van Gerven L (2022) Anatomical barriers against SARS-CoV-2 neuroinvasion at vulnerable interfaces visualized in deceased COVID-19 patients. *Neuron* 110:3919–3935.e6
57. Khan M, Yoo SJ, Clijsters M, Backaert W, Vanstapel A, Speleman K, Lietaer C, Choi S, Hether TD, Marcelis L, Nam A, Pan L, Reeves JW, Van Bulck P, Zhou H, Bourgeois M, Debaveye Y, De Munter P, Gunst J, Jorissen M, Lagrou K, Lorent N, Neyrinck A, Peetermans M, Thal DR, Vandenbrielle C, Wauters J, Mombaerts P, Van Gerven L (2021) Visualizing in deceased COVID-19 patients how SARS-CoV-2 attacks the respiratory and olfactory mucosae but spares the olfactory bulb. *Cell* 184:5932–5949.e15
58. Courtiol E, Wilson DA (2014) Thalamic olfaction: characterizing odor processing in the mediodorsal thalamus of the rat. *J Neurophysiol* 111:1274–1285
59. Dube M, Le Coupanec A, Wong AHM, Rini JM, Desforges M, Talbot PJ (2018) Axonal transport enables neuron-to-neuron propagation of human coronavirus OC43. *J Virol* 92:e00404-18
60. Tsukahara T, Brann DH, Datta SR (2023) Mechanisms of SARS-CoV-2-associated anosmia. *Physiol Rev* 103:2759–2766
61. Tyagi K, Rai P, Gautam A, Kaur H, Kapoor S, Suttee A, Jaiswal PK, Sharma A, Singh G, Barnwal RP (2023) Neurological manifestations of SARS-CoV-2: complexity, mechanism and associated disorders. *Eur J Med Res* 28:307
62. Steardo L Jr, Steardo L, Scuderi C (2023) Astrocytes and the psychiatric sequelae of COVID-19: what we learned from the pandemic. *Neurochem Res* 48:1015–1025
63. Almutairi MM, Sivandzade F, Albekairi TH, Alqahtani F, Cucullo L (2021) Neuroinflammation and its impact on the pathogenesis of COVID-19. *Front Med* 8:745789
64. Yinda CK, Port JR, Bushmaker T, Offei Owusu I, Purushotham JN, Avanzato VA, Fischer RJ, Schulz JE, Holbrook MG, Hebner MJ, Rosenke R, Thomas T, Marzi A, Best SM, de Wit E, Shaia C, van Doremalen N, Munster VJ (2021) K18-hACE2 mice develop respiratory disease resembling severe COVID-19. *PLoS Pathog* 17:e1009195
65. Kanno AI, Boraschi D, Leite LCC, Rodriguez D (2022) Recombinant BCG expressing the subunit 1 of pertussis toxin induces innate immune memory and confers protection against non-related pathogens. *Vaccines* 10:234
66. Rueda-Camino JA, Sendin-Martin V, Joya-Seijo MD, Angelina-Garcia M, Zamarro-Garcia C, Gimena-Rodriguez FJ, Barba-Martin R (2022) Plasma D-dimer value corrected by inflammatory markers in patients with SARS-CoV-2 infection: its prognostic value in the diagnosis of venous thromboembolism. *Med Clin* 158:265–269
67. Upmacis RK, Shen H, Benguigui LE, Lamon BD, Deeb RS, Hajjar KA, Hajjar DP (2011) Inducible nitric oxide synthase provides protection against injury-induced thrombosis in female mice. *Am J Physiol Heart Circ Physiol* 301:H617–624
68. Vieira-Alves I, Alves ARP, Souza NMV, Melo TL, Coimbra Campos LMC, Lacerda LSB, Queiroz-Junior CM, Andrade A, Barcelos LS, Teixeira MM, Costa VV, Cortes SF, Lemos VS (2023) TNF/iNOS/NO pathway mediates host susceptibility to endothelial-dependent circulatory failure and death induced by betacoronavirus infection. *Clin Sci* 137:543–559
69. Mason RJ (2020) Pathogenesis of COVID-19 from a cell biology perspective. *Eur Respir J* 55:2000607
70. de Bree LCJ, Koeken V, Joosten LAB, Aaby P, Benn CS, van Crevel R, Netea MG (2018) Non-specific effects of vaccines: current evidence and potential implications. *Semin Immunol* 39:35–43
71. Shann F (2015) Editorial Commentary: different strains of Bacillus Calmette–Guerin vaccine have very different effects on tuberculosis and on unrelated infections. *Clin Infect Dis* 61:960–962
72. Counoupas C, Johansen MD, Stella AO, Nguyen DH, Ferguson AL, Aggarwal A, Bhattacharyya ND, Grey A, Hutchings O, Patel K, Siddiquee R, Stewart EL, Feng CG, Hansbro NG, Palendira U, Steain MC, Saunders BM, Low JKK, Mackay JP, Kelleher AD, Britton WJ, Turville SG, Hansbro PM, Triccas JA (2021) A single dose, BCG-adjuvanted COVID-19 vaccine provides sterilising immunity against SARS-CoV-2 infection. *NPJ Vaccines* 6:143
73. Kang A, Ye G, Singh R, Afkhami S, Bavananthasivam J, Luo X, Vaseghi-Shanjani M, Aleithan F, Zganiacz A, Jeyanathan M, Xing Z (2023) Subcutaneous BCG vaccination protects against streptococcal pneumonia via regulating innate immune responses in the lung. *EMBO Mol Med* 15:e17084
74. Yang JH, Yang MS, Kim DM, Kim B, Tark D, Kang SM, Lee GH (2023) Delta (B16172) variant of SARS-CoV-2 induces severe neurotropic patterns in K18-hACE2 mice. *Sci Rep* 13:3303
75. Ziogas A, Netea MG (2022) Trained immunity-related vaccines: innate immune memory and heterologous protection against infections. *Trends Mol Med* 28:497–512
76. Moreo E, Jarit-Cabanillas A, Robles-Vera I, Uranga S, Guerrero C, Gomez AB, Mata-Martinez P, Minute L, Araujo-Voces M, Felgueres MJ, Estes G, Uranga-Murillo I, Arias M, Pardo J, Martin C, Vales-Gomez M, Del Fresno C, Sancho D, Aguilo N (2023) Intravenous administration of BCG in mice promotes natural killer and T cell-mediated antitumor immunity in the lung. *Nat Commun* 14:6090
77. Jeljeli M, Riccio LGC, Doridot L, Chene C, Nicco C, Chouzenoux S, Deletang Q, Allanore Y, Kavian R, Batteux F (2019) Trained immunity modulates inflammation-induced fibrosis. *Nat Commun* 10:5670

Publisher's Note

Springer Nature remains neutral with regard to jurisdictional claims in published maps and institutional affiliations.